The metastasis suppressor NDRG1 down-regulates the epidermal growth factor receptor via a lysosomal mechanism by up-regulating mitogen-inducible gene 6

Received for publication, October 25, 2018, and in revised form, January 9, 2019 Published, Papers in Press, January 24, 2019, DOI 10.1074/jbc.RA118.006279

Sharleen V. Menezes, Zaklina Kovacevic[1,2], and Des R. Richardson[1,3]

From the Molecular Pharmacology and Pathology Program, Department of Pathology and Bosch Institute, Medical Foundation Building (K25), University of Sydney, Sydney, New South Wales, 2006 Australia

Edited by Eric R. Fearon

The metastasis suppressor, N-Myc downstream-regulated gene-1 (NDRG1) inhibits a plethora of oncogenic signaling pathways by down-regulating the epidermal growth factor receptor (EGFR). Herein, we examined the mechanism involved in NDRG1-mediated EGFR down-regulation. NDRG1 overexpression potently increased the levels of mitogen-inducible gene 6 (MIG6), which inhibits EGFR and facilitates its lysosomal processing and degradation. Conversely, silencing *NDRG1* in multiple human cancer cell types decreased MIG6 expression, demonstrating the regulatory role of NDRG1. Further, NDRG1 overexpression facilitated MIG6–EGFR association in the cytoplasm, possibly explaining the significantly (p <0.001) increased half-life of MIG6 from 1.6 ± 0.2 h under control conditions to 7.9 ± 0.4 h after NDRG1 overexpression. The increased MIG6 levels enhanced EGFR co-localization with the late endosome/lysosomal marker, lysosomal-associated membrane protein 2 (LAMP2). An increase in EGFR levels after *MIG6* silencing was particularly apparent when NDRG1 was overexpressed, suggesting a role for MIG6 in NDRG1-mediated down-regulation of EGFR. Silencing phosphatase and tensin homolog (*PTEN*), which facilitates early to late endosome maturation, decreased MIG6, and also increased EGFR levels in both the presence and absence of NDRG1 overexpression. These results suggest a role for PTEN in regulating MIG6 expression. Anti-tumor drugs of the di-2-pyridylketone thiosemicarbazone class that activate NDRG1 expression also potently increased MIG6 and induced its cytosolic co-localization with NDRG1. This was accompanied by a decrease in activated and total EGFR levels and its redistribution to late endosomes/lysosomes. In conclusion, NDRG1 promotes EGFR down-regulation through the EGFR inhibitor MIG6, which leads to late endosomal/lysosomal processing of EGFR.

N-Myc downstream regulated gene 1 (NDRG1)[4] is a potent metastasis suppressor in many tumor cell types, including pancreatic (1, 2), breast (3), prostate (4), and colonic cancer (5). The *NDRG1* gene is found on chromosome 8q24.3 (6), which encodes a 394–amino acid protein of the NDRG1 family that includes four members, NDRG1–4 (7–9). Considering this family of proteins, NDRG1 is unique in that it has three tandem (GTRSRSHTSE) repeat sequences near its C terminus end (9). The NDRG1 protein can be induced by stress stimuli, including cellular iron depletion and hypoxia through hypoxia-inducible factor-1α (HIF-1α)–dependent and –independent mechanisms (10, 11).

The surprisingly broad and promiscuous anti-tumor activity of NDRG1 includes its ability to inhibit oncogenic PI3K/AKT (12, 13), ERK (13), RAS (12), TGF-β (13, 14), WNT (15, 16), Src (17), ROCK/pMLC2 (18), and NF-κB (19) signaling. Studies from our laboratory recently indicate that the ability of NDRG1 to inhibit these pathways is because of its ability to down-regulate the epidermal growth factor receptor (EGFR) (20, 21) that plays a role as a master regulator of diverse downstream signaling pathways. However, the exact mechanism(s) involved in terms of the interaction between EGFR and NDRG1 remain unclear. The anti-oncogenic effector function of NDRG1 has been convincingly documented *in vitro* (14, 21) and *in vivo* (4, 16), making this molecule an important therapeutic target (10, 16, 22).

The EGFR is a membrane-bound tyrosine kinase that plays a key role in critical cellular programs, including survival, proliferation, and metastasis, with spurious EGFR activation being

This work was supported by National Health and Medical Research Council of Australia (NHMRC) Project Grant 1060482 (to D. R. R. and Z. K.), Priority-driven Collaborative Cancer Research Scheme Grant 1086449, Cure Cancer Australia Foundation, and Cancer Australia (to Z. K.). This work was also supported by an Australian Postgraduate Award from the University of Sydney (to S. V. M), an NHMRC Senior Principal Research Fellowship (1062607) (to D. R. R.), an NHMRC Peter Doherty Early Career Fellowship (1037323) (to Z. K), a Cancer Institute New South Wales Early Career Fellowship (12-ECF2–17), an NHMRC RD Wright Fellowship (APP1140447), and a Cancer Institute New South Wales Career Development Fellowship (CDF171126). The authors declare that they have no conflicts of interest with the contents of this article.

This article contains Figs. S1–S5.

[1] These authors contributed equally to this work as senior authors.

[2] To whom correspondence may be addressed. Tel.: 61-2-9036-3026; E-mail: zaklina.kovacevic@sydney.edu.au.

[3] To whom correspondence may be addressed. Tel.: 61-2-9036-3026; E-mail: d.richardson@med.usyd.edu.au.

[4] The abbreviations used are: NDRG1, N-Myc downstream regulated gene-1; HIF-1α, hypoxia-inducible factor-1α; ERK, extracellular signal-regulated kinase; TGF, transforming growth factor; EGFR, epidermal growth factor receptor; EGF, epidermal growth factor; HIF-1α, hypoxia-inducible factor-1α; MIG6, mitogen-inducible gene 6; RALT, receptor-associated late transducer; DpT, di-2-pyridylketone thiosemicarbazone; Dp44mT, di-2-pyridylketone 4,4-dimethyl-3-thiosemicarbazone; DpC, di-2-pyridylketone 4-cyclohexyl-4-methyl-3-thiosemicarbazone; DFO, desferrioxamine; LAMP2, lysosome-associated membrane protein 2; VC, vector control; NH_4Cl, ammonium chloride; CH_3NH_2, methylamine; EEA1, early endosomal antigen 1; PTEN, phosphatase and tensin homolog; Bp2mT, 2-benzoylpyridine 2-methyl-3-thiosemicarbazone.

© 2019 Menezes et al. Published under exclusive license by The American Society for Biochemistry and Molecular Biology, Inc.

involved in cellular transformation (23). EGFR activation is prevented by self-inhibitory constraints imposed on the extracellular ligand–binding domain (24) and its intracellular catalytic domain (25). These constraints are liberated by epidermal growth factor (EGF) binding that drives dimerization, allosteric activation of the kinase, EGFR autophosphorylation and downstream signaling (24, 26). Interestingly, EGFR signaling is negatively controlled by 1) multiple inducible inhibitors (27, 28) and 2) receptor-mediated endocytosis, leading to its internalization and degradation by the lysosomal compartment (29).

The mitogen-inducible gene 6 (MIG6), also known as the receptor-associated late transducer (RALT), or ERBB receptor feedback inhibitor 1 (ERRFI), is a transcriptionally induced EGFR inhibitor that is also a tumor suppressor (30, 31). MIG6 is a cytoplasmic protein (32) that binds to the EGFR dimer interface, preventing the formation of asymmetric catalytic dimers, locking it into a catalytically inactive conformation (26). Significantly, MIG6 can also induce internalization and degradation of EGFR via a lysosomal mechanism, which integrates its ability to act to inhibit EGFR catalytic activity and down-regulate its levels (33).

A recently described group of anti-cancer agents of the di-2-pyridylketone thiosemicarbazone (DpT) class potently inhibit tumor growth and metastasis at least in part by their ability to up-regulate NDRG1 through a mechanism involving intracellular iron binding (10, 16, 22, 34–37). The first lead agent of this class of agents, di-2-pyridylketone 4,4-dimethyl-3-thiosemicarbazone (Dp44mT), leads to the marked up-regulation of NDRG1 in many tumor cell types (10, 35). An analog of Dp44mT, namely di-2-pyridylketone 4-cyclohexyl-4-methyl-3-thiosemicarbazone (DpC) (36), also potently up-regulates NDRG1 (35). This agent possesses marked anti-tumor activity against a variety of belligerent tumors *in vitro* and *in vivo* (35, 36, 38, 39) and has entered Phase I clinical trials for the treatment of advanced and resistant cancer (40). Of interest, agents that bind intracellular iron, such as desferrioxamine (DFO), can also up-regulate MIG6 (41), which could be mediated through an iron-responsive increase in HIF-1α levels, which is known to transcriptionally up-regulate MIG6 (42).

Herein, we demonstrate that the mechanism involved in EGFR down-regulation mediated by NDRG1 occurs through it potently increasing MIG6 levels, which both directly inhibits EGFR and facilitates its lysosomal degradation. NDRG1 was shown to increase EGFR internalization and co-localization with the late endosome/lysosomal marker, lysosome-associated membrane protein 2 (LAMP2). Moreover, MIG6 and NDRG1 were demonstrated to be associated and co-localized in the cytoplasm with NDRG1 overexpression increasing MIG6 half-life. Increased EGFR levels after *MIG6* silencing was particularly apparent with NDRG1 overexpression, suggesting a role for MIG6 in the NDRG1-mediated down-regulation of EGFR. As an innovative therapeutic targeting strategy, novel anti-cancer drugs of the DpT class that up-regulate NDRG1 expression (10, 35) increased MIG6 and induced its co-localization with NDRG1 in the cytoplasm. This led to a decrease in activated and total EGFR levels as well as the redistribution of EGFR to LAMP2-stained late endosomes/lysosomes. In conclusion, NDRG1 promotes MIG6-mediated EGFR down-regulation by lysosomal processing, and this could be important for understanding the broad ability of NDRG1 expression to inhibit a plethora of oncogenic signaling pathways.

Results

NDRG1 overexpression up-regulates MIG6 and decreases EGFR total levels and EGFR phosphorylation at Tyr-1068

Our laboratory previously demonstrated that NDRG1 inhibited a plethora of oncogenic signaling pathways by down-regulating a key upstream regulator, EGFR (21). The aim of the current study was to dissect the mechanism by which NDRG1 decreased EGFR expression. Therefore, considering the integral role of MIG6 in this process (33), it was deemed important to investigate the potential effect of NDRG1 on MIG6 expression and its ability to down-regulate EGFR.

Initially, PANC-1 vector control (VC) cells and cells stably transfected to overexpress NDRG1 (Fig. 1*A*; *N1*) were used as they have been well-characterized in our laboratory regarding the ability of NDRG1 to inhibit multiple oncogenic signaling pathways (12) by down-regulating EGFR (21). First, PANC-1 VC and N1 cells were incubated in the presence and absence of the ligand EGF (10 ng/ml) for 2, 5, and 10 min (Fig. 1*A*). Examining NDRG1 expression in VC cells, two endogenous NDRG1 bands were apparent at 41 and 46 kDa that did not significantly alter upon incubation with EGF relative to the control. The densitometry of NDRG1 shown in Fig. 1*A* represents the total of all bands. These bands are consistent with the different isoforms of NDRG1 reported previously that may be the result of NDRG1 processing, cleavage, or differential phosphorylation (43, 44). The overexpression of NDRG1 in the N1 clone resulted in a third exogenous band at 48 kDa that was above the endogenous 41- and 46-kDa bands (Fig. 1*A*), which corresponds to NDRG1 with its FLAG-tag (12). The expression of total NDRG1 in the N1 clone was significantly ($p < 0.001$) greater than that of VC cells at all incubation times (Fig. 1*A*).

Total EGFR levels in PANC-1 VC cells were slightly decreased by the addition of EGF as a function of incubation time relative to the control (Fig. 1*A*). Overexpression of NDRG1 in control PANC-1 N1 cells resulted in a significant ($p < 0.01$) decrease in EGFR compared with the VC control. This decrease in EGFR expression in N1 cells relative to its VC counterparts became more apparent as a function of incubation time with EGF, in agreement with our previous studies (21). In contrast, *EGFR* mRNA levels were not affected by NDRG1 overexpression in the absence and presence of EGF, as demonstrated using two different NDRG1-overexpressing clones, namely N1 and N2 cells (Fig. S1*B*). Relative to the effect observed with NDRG1 overexpression, silencing this molecule resulted in up-regulation of EGFR in PANC-1 cells (Fig. S1*C*), as we also demonstrated in CFPAC-1 cells (21). Furthermore, silencing NDRG1 in HT-29 colon cancer cells also resulted in a similar up-regulation of EGFR (Fig. S1*C*).

In terms of the effect of NDRG1 expression on EGFR activation, treatment of VC cells with EGF caused pronounced and significant ($p < 0.001$) increase in pEGFR levels at Tyr-1068 at incubations from 2 to 10 min relative to the 0 min time point (Fig. 1*A*). Of note, the pEGFR phosphorylation at Tyr-1068 has

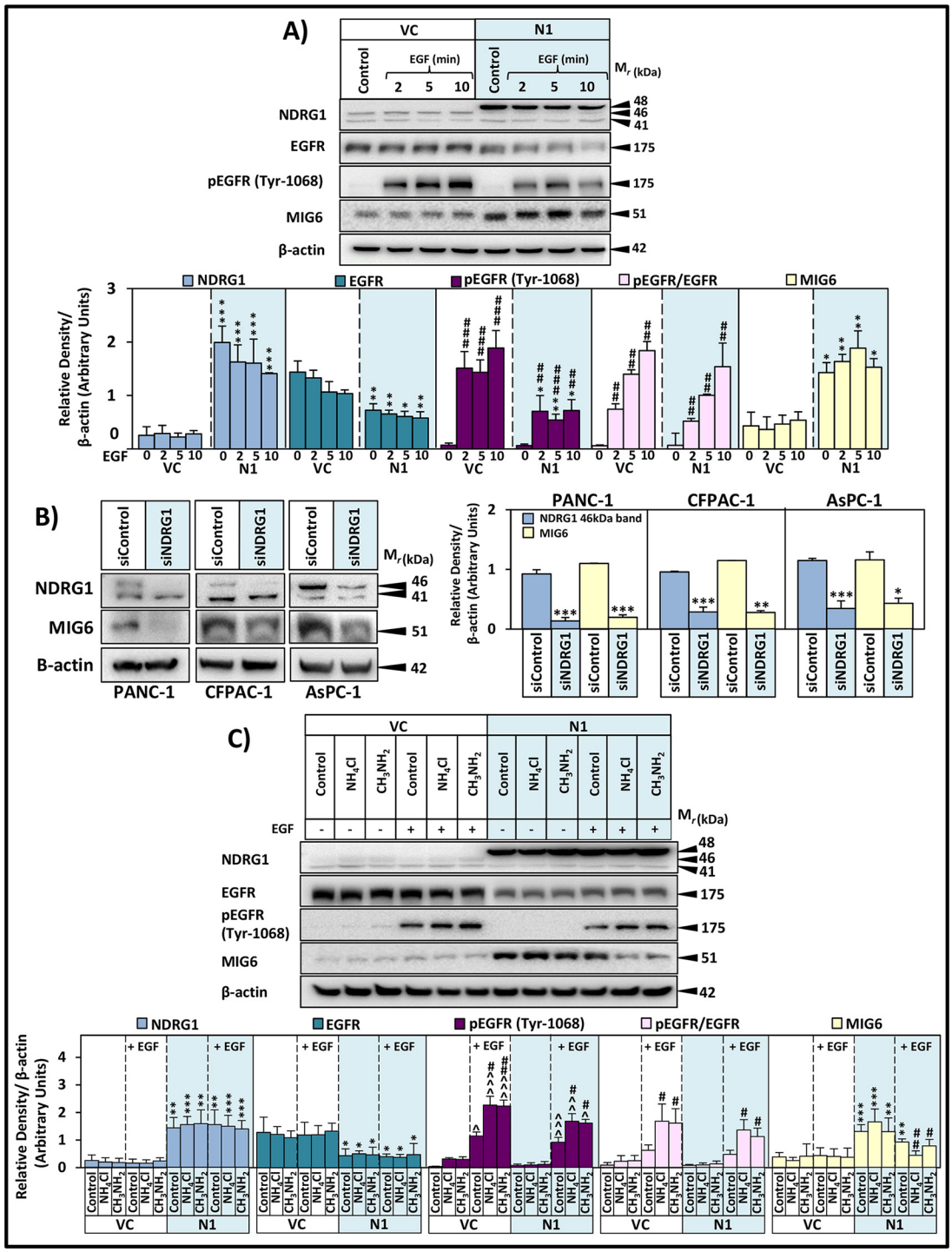

Figure 1. *A* and *B*, NDRG1 overexpression enhances MIG6 levels (*A*), with this effect being reversed (*B*) when NDRG1 is silenced. *C*, NDRG1's effect on the decreasing activated EGFR and up-regulating MIG6 is reversed in the presence of the lysosomotropic agents NH_4Cl and CH_3NH_2. PANC-1 vector control (VC) and NDRG1-overexpressing (N1) cells were (*A*) incubated in the presence and absence of the ligand EGF (10 ng/ml) for 2, 5, and 10 min at 37 °C, and (*C*) with NH_4Cl and CH_3NH_2, and in combination with EGF in the last 10 min of treatment at 37 °C. *B*, PANC-1, CFPAC-1, and AsPC-1 VC cells were transiently transfected with *NDRG1* siRNA (siNDRG1) or nonspecific control siRNA (siControl) under the conditions described in "Materials and Methods." Total cell protein was extracted and electrophoresed on a 10% SDS-PAGE gel followed by Western blot analysis to detect (*A*) and (*C*) NDRG1, EGFR, pEGFR (Tyr-1068), and MIG6 expression, and (*B*) NDRG1 and MIG6 expression. β-actin was used as a protein-loading control. Results are mean ± S.D. ($n = 3$). *A* and *C*, *, $p < 0.05$; **, $p < 0.01$; ***, $p < 0.001$ denotes statistical significance comparing NDRG1 overexpressing cells relative to VC cells. #, $p < 0.05$; ##, $p < 0.01$; ###, $p < 0.001$ denote statistical significance comparing the cells to their respective control within VC or N1 cells. ∧, $p < 0.05$; ∧∧, $p < 0.01$; ∧∧∧, $p < 0.001$ denote statistical significance comparing the control cells to EGF-treated cells. *B*, *, $p < 0.05$; **, $p < 0.01$; ***, $p < 0.001$ denotes statistical significance comparing siControl cells relative to siNDRG1 cells.

been demonstrated to activate the Ras/mitogen activated protein kinase signaling pathway, which is implicated in uncontrolled cancer growth (45).

The pEGFR (Tyr-1068) levels were also significantly ($p < 0.001–0.01$) increased in N1 cells upon incubation with EGF relative to the 0 min control time point (Fig. 1*A*). This was

significantly (p <0.01–0.05) less marked relative to that observed in VC cells at all time points. In addition, the ratio of pEGFR to total EGFR was markedly and significantly (p <0.01) increased with increasing EGF incubation time relative to the 0 min control for both VC and N1 cells (Fig. 1*A*). However, there was no (p >0.05) significant difference in these ratios at each incubation time when comparing VC to N1 cells. This is in agreement with our previous investigation (21), whereby NDRG1 was able to decrease pEGFR by reducing total EGFR levels, rather than specifically decreasing EGFR phosphorylation.

Examining MIG6 expression in VC cells, incubation with EGF had no significant (p >0.05) effect relative to the control (Fig. 1*A*). Interestingly, NDRG1 expression in N1 cells resulted in significantly (p <0.01–0.05) higher levels of MIG6 relative to the VC at all time points, with EGF having no appreciable effect relative to the 0 min control. Examination of mRNA levels of *NDRG1* and *MIG6*, demonstrated that in contrast to the marked up-regulation of *NDRG1* mRNA in N1 cells relative to VC cells, there was no significant (p >0.05) alteration in *MIG6* mRNA levels in the N1 cell type (Fig. S1*D*). This observation suggests that the effect of NDRG1 on MIG6 was mediated by posttranscriptional regulation. Collectively, the ability of NDRG1 to down-regulate EGFR and decrease pEGFR (Tyr-1068) could be because of its effect on up-regulating protein levels of the EGFR inhibitor MIG6.

To confirm the role of NDRG1 in regulating MIG6 protein levels (Fig. 1*A*), the effect of *NDRG1* silencing (siNDRG1) relative to its negative control siRNA (siControl) was assessed in three different pancreatic cancer cell lines, namely PANC-1, CFPAC-1, and AsPC-1 (Fig. 1*B*). In all cell types, effective *NDRG1* silencing was observed, resulting in marked and significant (p <0.001) down-regulation of the NDRG1 46-kDa band, but not the 41-kDa band (Fig. 1*B*). This is in good agreement with previous studies (12, 14, 43), and indicates the presence of NDRG1 isoforms, with the lower band being consistent with a long-lived cleaved isoform (43, 44). The upper NDRG1 band has been suggested to be the active form of the protein for metastasis suppression, as it is potently up-regulated by drugs that inhibit tumor growth and block metastasis (16, 35, 43). Moreover, silencing of the top NDRG1 band prevents the ability of NDRG1 to act on downstream effectors (*e.g.* E-cadherin and β-catenin) (14) involved in preventing the epithelial mesenchymal transition and metastasis. The down-regulation of the upper NDRG1 band by siRNA is important to achieve experimentally in terms of preventing its downstream anti-oncogenic functions. In fact, silencing *NDRG1* resulted in a significant (p <0.001–0.05) decrease in MIG6 expression in all three cell types (Fig. 1*B*). An additional siRNA of NDRG1 was also examined in PANC-1 cells, resulting in a marked decrease in MIG6 expression relative to the control (Fig. S1*E*). Hence, the regulation of MIG6 occurs through the differential expression of NDRG1.

Lysosomotropic agents that prevent lysosomal acidification perturb pEGFR (Tyr-1068) and MIG6 levels

It has been established that a major process by which EGFR undergoes degradation is through trafficking to lysosomes (29, 33, 46, 47). Considering this, it was important to investigate whether NDRG1 promoted EGFR processing through this mechanism. In these studies, PANC-1 cells were treated in the absence and presence of the well-characterized lysosomotropic agents ammonium chloride (NH_4Cl; 15 mM) or methylamine (CH_3NH_2; 15 mM) that inhibit lysosomal acidification and function (48) for 24 h/37 °C, followed by treatment with EGF (10 ng/ml) for the last 10 min/37 °C of the incubation (Fig. 1*C*).

For VC or N1 cells, incubation with NH_4Cl or CH_3NH_2 in the presence or absence of EGF had no significant (p >0.05) effect on NDRG1 expression relative to the control. However, as observed for Fig. 1*A*, N1 cells had significantly (p <0.001–0.01) higher levels of NDRG1 compared with VC cells (Fig. 1*C*). Examining total EGFR expression, in VC cells, NH_4Cl or CH_3NH_2 had no significant (p >0.05) effect in the presence or absence of EGF. Under all incubation conditions in N1 cells, EGFR expression was significantly (p <0.05) decreased in the presence and absence of EGF. Treatment of N1 cells with NH_4Cl or CH_3NH_2 had no significant (p >0.05) effect on EGFR levels in the presence of EGF relative to the N1 control without EGF (Fig. 1*C*).

When assessing the levels of pEGFR (Tyr-1068) in VC cells, the addition of EGF to VC cells caused a significant (p <0.001–0.05) increase in the levels pEGFR at Tyr-1068 relative to the control under all conditions (Fig. 1*C*), which is expected in this cell type (21). This response was markedly enhanced when EGF was added to VC cells incubated with NH_4Cl or CH_3NH_2, there being a pronounced and significant (p <0.01–0.05) increase in pEGFR (Tyr-1068) relative to the VC control (Fig. 1*C*). The increase in pEGFR (Tyr-1068) levels after incubation with these lysosomotropic agents is probably because of inhibition of the degradation of the phosphorylated receptor, as demonstrated for these agents by others (49). However, examining N1 cells, pEGFR (Tyr-1068) levels were lower under all conditions relative to their VC counterparts (Fig. 1*C*). Upon incubation of N1 cells with EGF, there was a significant (p <0.001–0.05) increase in pEGFR (Tyr-1068) under all conditions relative to N1 cells in the absence of EGF. As observed for VC cells, incubation of N1 cells with NH_4Cl or CH_3NH_2 significantly (p <0.05) increased pEGFR (Tyr-1068) in the presence of EGF relative to the EGF control (Fig. 1*C*). Again, this could be because of the inhibited degradation of the phosphorylated receptor by these agents leading to higher levels (49).

Furthermore, the ratios of pEGFR/EGFR were calculated in both VC and N1 cells with and without treatment with NH_4Cl or CH_3NH_2 (Fig. 1*C*). It was demonstrated that in the absence of EGF, there was a slight increase in the pEGFR/EGFR ratio upon incubation of VC cells with the lysosomotropic agents. Upon the addition of EGF to VC cells, the pEGFR/EGFR ratio was increased compared with their untreated counterparts (Fig. 1*C*). Further, the addition of lysosomotropic agents to VC cells in the presence of EGF caused a marked and significant (p <0.05) increase in the ratio relative to the EGF-treated control. Similar to VC cells, the effect of the lysosomotropic agents in the presence of EGF caused a significant (p <0.05) increase in the pEGFR/EGFR ratio relative to the control in N1 cells (Fig. 1*C*). These results demonstrate that inhibiting lysosomal degradation increases pEGFR, which is able to accumulate because of its inability to be degraded via the lysosome.

Examination of MIG6 levels demonstrated that VC cells incubated without or with lysosomotropic agents in the absence or presence of EGF were not significantly ($p > 0.05$) altered relative to the controls (Fig. 1*C*). On the other hand, in N1 cells in the absence of EGF, MIG6 levels were significantly ($p < 0.001–0.01$) enhanced by NDRG1 under all conditions relative to the respective VC controls. Although NH_4Cl and CH_3NH_2 had no significant effect on MIG6 expression in the absence of EGF, these agents significantly ($p < 0.01–0.05$) decreased MIG6 in the presence of EGF in N1 cells (Fig. 1*C*). Together, these data indicate that the lysosomotropic agents are perturbing pEGFR (Tyr-1068) and MIG6 levels, suggesting potential lysosomal processing that was then investigated further below.

NDRG1 overexpression increases EGFR internalization and co-localization with the early endosomal marker EEA1 and the late endosome/lysosomal marker LAMP2

Considering the lysosomal process that down-regulates EGFR (50, 51), the results above in Fig. 1*C* suggest lysosomal involvement in the role of NDRG1 in decreasing EGFR expression and activation. To examine this further, PANC-1 VC and N1 cells were incubated in the presence and absence of EGF (10 ng/ml) for 10 min/37 °C (Fig. 2*A*). Cells were then assessed by immunofluorescence using confocal microscopy and stained for EGFR (*red*), the well-characterized early endosomal marker, EEA1 (*green*) (52) and DAPI (*blue*) for the nucleus.

Considering first nuclear DAPI staining, some slight, but not significant, differences in nuclear size were apparent upon close examination of the images taken. This is probably because nuclear size does naturally vary depending on the stage of the cell cycle (53). As expected in VC control cells, EGFR showed strong red staining on the membrane with some intracellular staining as well (Fig. 2*A*). In VC cells incubated with EGF, EGFR expression was again evident on the plasma membrane and intracellularly (Fig. 2*Ai*). In contrast, in control N1 cells overexpressing NDRG1 in the presence and absence of EGF, EGFR levels were overall significantly ($p < 0.01$) lower. These findings are in agreement with the Western blot studies in Fig. 1, *A* and *C*. In addition, N1 cells incubated in the presence or absence of EGF resulted in greater intracellular clustering of EGFR relative to VC cells (Fig. 2*A*). Assessing EEA1 expression in both VC and N1 cells under all conditions, there was no significant ($p > 0.05$) alteration in the intensity of this marker, which was uniformly distributed in the cytoplasm (Fig. 2*A*).

Quantification of co-localization demonstrated increased co-localization of EGFR and EEA1 being evident in yellow puncta in N1 cells treated with EGF (Fig. 2*A*). This co-localization was significantly ($p < 0.001$) greater in the presence of EGF relative to the VC counterpart treated with EGF (Fig. 2*Aii*). Furthermore, examining the extent of this association using Pearson's correlation coefficient (r), higher co-localization was evident in N1 EGF-treated cells ($r = 0.699$) compared with EGF-treated VC cells ($r = 0.346$; Fig. 2*A*), suggesting a role for NDRG1 in trafficking and sorting of EGFR into the early endosomal compartment.

After being sorted to the endosome, EGFR can be transported to the lysosome for degradation (51). In order to further explore the association of NDRG1 with EGFR and the lysosome, the localization of these proteins was also examined (Fig. 2*B*). Similarly to Fig. 2*A*, PANC-1 VC and N1 cells were incubated with EGF (10 ng/ml)/10 min at 37 °C, and then examined for the distribution of EGFR, DAPI, and the late endosome/lysosomal marker LAMP2 (shown in *green*) (54). Examining EGFR, similar effects were observed in terms of NDRG1 expression to that observed in Fig. 2*A*, with EGFR intensity being significantly ($p < 0.05$) decreased in N1 cells relative to VC cells (Fig. 2*Bi*). Furthermore, intracellular clustering of EGFR was evident in N1 cells relative to their VC counterparts (Fig. 2*B*). In contrast to EEA1 expression (Fig. 2*A*), LAMP2 distribution became markedly more clustered in the N1 cells regardless of EGF and appeared perinuclear (Fig. 2*B*). However, the overall intensity of LAMP2 in N1 cells was not significantly ($p > 0.05$) changed relative to its VC counterparts (Fig. 2*Bi*), suggesting altered distribution rather than expression.

In VC cells in the presence and absence of EGF, minimal co-localization was observed between LAMP2 and EGFR ($r = 0.436–0.445$) (Fig. 2*Bii*). However, examining N1 cells, there was an increase in intracellular EGFR and the clustering of LAMP2-stained late endosomes/lysosomes, as well as co-localization of EGFR and LAMP2 (Fig. 2*B*). Quantification analysis showed that in N1 cells, co-localization of EGFR and LAMP2 occurred in the presence and absence of EGF and was significantly ($p < 0.01$) higher than that observed in VC cells (Fig. 2*Bii*). This was further documented by the increased Pearson's correlation coefficients calculated in N1 cells ($r = 0.768–0.813$) compared with VC cells ($r = 0.436–0.445$). Together, these findings in Fig. 2, *A* and *B*, indicate the role of NDRG1 in fostering the trafficking and sorting of EGFR to the early endosome, followed by the lysosome. Of note, in contrast to the marked co-localization between LAMP2 and EGFR observed in Fig. 2*B*, no appreciable co-localization was observed between NDRG1 and EEA1 ($r = 0.403–0.516$) (Fig. S2*A*), NDRG1 and LAMP2 ($r = 0.441–0.493$) (Fig. S2*B*), MIG6 and EEA1 ($r = 0.357–0.478$) (Fig. S2*C*), or MIG6 and LAMP2 ($r = 0.356–0.505$) (Fig. S2*D*).

Inhibition of the proteasome by MG132, but not lactacystin, increases levels of pEGFR (Tyr-1068)

Although the involvement of the proteasome in the degradation of EGFR is not completely understood, there is evidence to suggest its role in inhibiting EGFR signaling. To therefore assess the possible involvement of proteasomal degradation in the NDRG1-mediated inhibition of EGFR expression and signaling, the well-characterized proteasomal inhibitors, MG132 or lactacystin, were used. PANC-1 cells were incubated with MG132 (2.5 μM) or lactacystin (5 μM) for 24 h/37 °C, with EGF (10 ng/ml) being added in the last 10 min of the incubation (Fig. 3).

Incubation with MG132 resulted in the detection of a 47-kDa NDRG1 band in VC cells which is slightly above the 46-kDa NDRG1 band observed in VC cells in the absence of MG132 (Fig. 3*A*). As reported above (Fig. 1*A*), the 48-kDa NDRG1 band was prominent in N1 cells (Fig. 3*A*). Upon incubation of N1 cells with MG132, there was marked and significant ($p < 0.05$) potentiation of this 48-kDa NDRG1

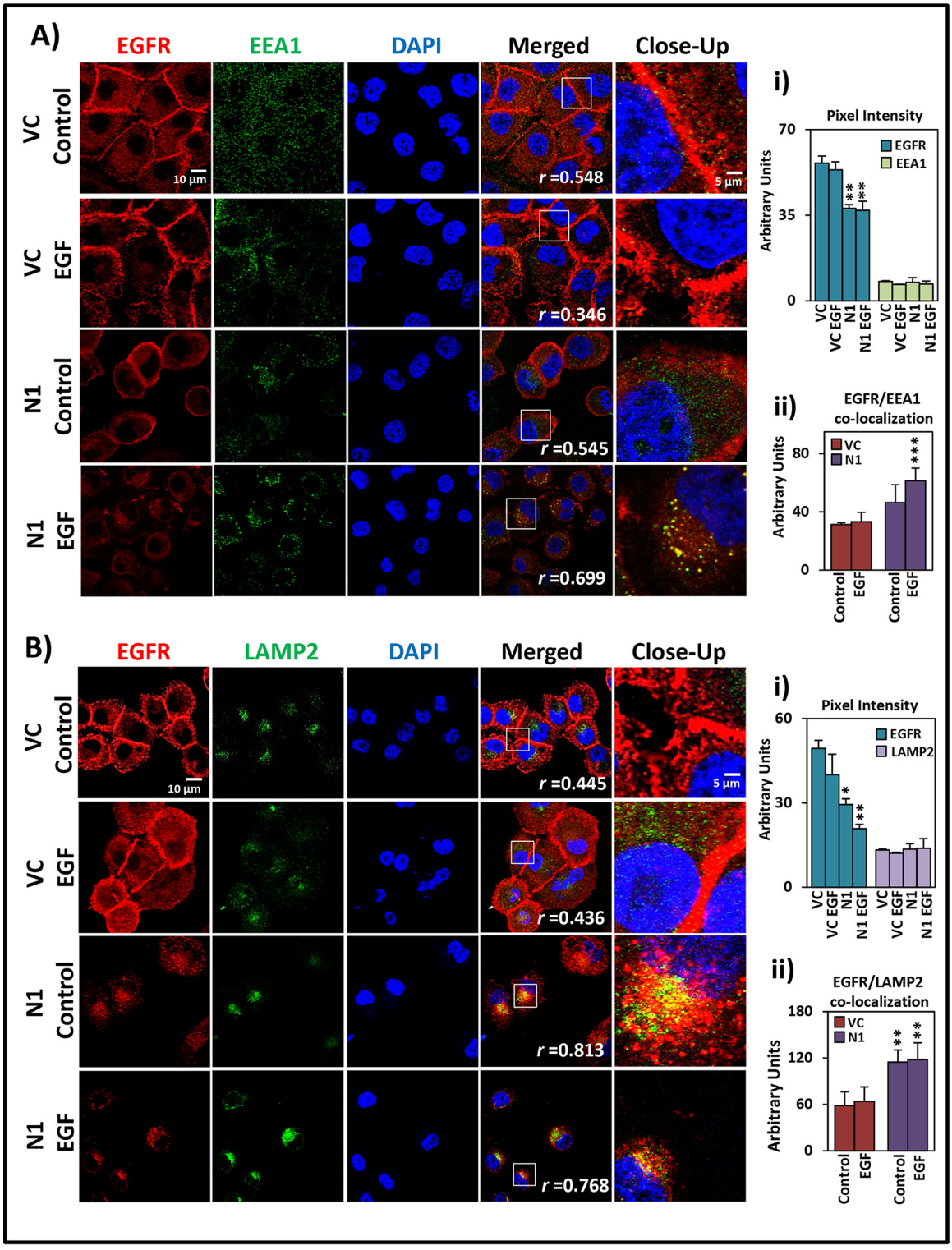

Figure 2. *A* and *B*, NDRG1 increases EGFR internalization and co-localization with (*A*) the early endosome marker EEA1 in the presence of EGF and (*B*) the late endosome/lysosome marker LAMP2 in the absence and presence of EGF in PANC-1 cells. VC or N1 PANC-1 cells were incubated with either control medium or medium containing EGF (10 ng/ml) for 10 min/37 °C. Immunofluorescence images show staining for EGFR (*red*), DAPI for nuclei (*blue*) and (*A*) EEA1 (*green*) or (*B*) LAMP2 (*green*). All images were taken with a 63× objective and at the same exposure time using AxioVision™ software. Images are representative from three experiments performed. *A* and *B*, quantification of (*Ai*) pixel intensity of EGFR or EEA1, (*Aii*) co-localization of EGFR and EEA1, (*Bi*) pixel intensity of EGFR and LAMP2, and (*Bii*) co-localization of EGFR and LAMP2. The quantification was performed using ImageJ software and expressed as mean ± S.D. (three experiments) where *, $p < 0.05$; **, $p < 0.01$; ***, $p < 0.001$ relative to the respective control. Pixel intensity and co-localization analysis utilized a total of 40–65 cells over three experiments. *A* and *B*, the *scale bar* in the *bottom right-hand corner* of the first image represents 10 μm and is the same across all images, except the *close-up panel*, where the *scale bar* is 5 μm.

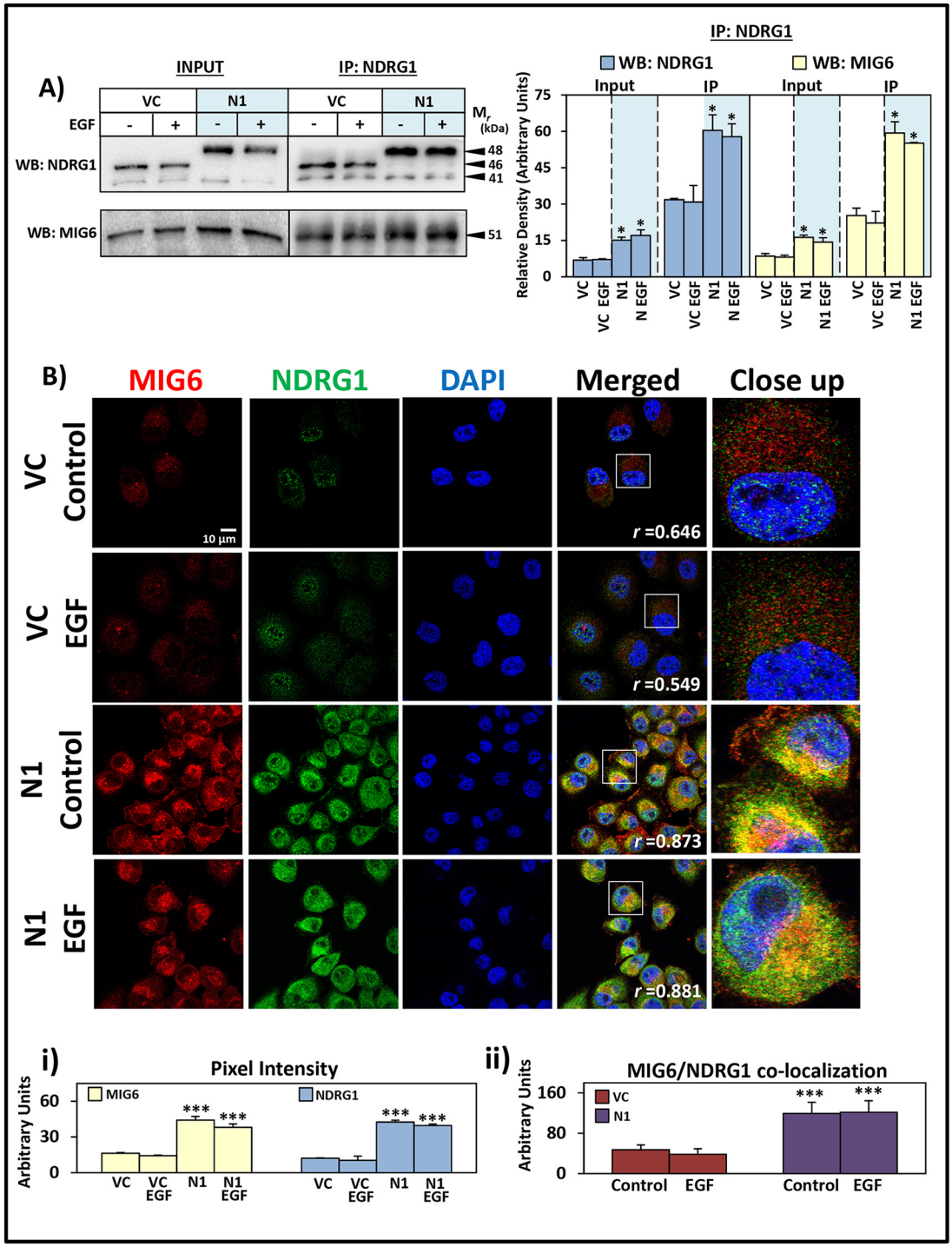

Figure 3. NDRG1 overexpression increases the association of MIG6 and NDRG1. *A* and *B*, PANC-1 VC or N1 cells were incubated with control media or media containing EGF (10 ng/ml; 10 min/37 °C) and examined via (*A*) co-immunoprecipitation or (*B*) immunofluorescence. *A*, NDRG1 was immunoprecipitated and then Western blotting performed to detect NDRG1 and MIG6 expression. Input lysates of the total protein were included for comparison with immunoprecipitated lysates for each sample. Western blots are typical of three independent experiments, with densitometric analysis representing mean ± S.D. (n = 3). Relative to untreated vector control cells, *, $p < 0.05$ in the respective condition. *B*, under the same conditions, immunofluorescence images show staining for MIG6 (*red*), NDRG1 (*green*), and DAPI for nuclei (*blue*). All images were taken with a 63× objective and at the same exposure time using AxioVision™ software. Images are representative from three experiments performed. Pixel intensity of (*Bi*) MIG6 and NDRG1 and (*Bii*) MIG6/NDRG1 co-localization was calculated using ImageJ Software, whereby ***, $p < 0.001$ denotes significance comparing each condition to control cells. Pixel intensity and co-localization analysis utilized a total of 30–60 cells over three experiments. *B*, the *scale bar* in the *bottom right-hand corner* of the first image represents 10 μm and is the same across all images, except the *close-up panel*, where the *scale bar* is 5 μm.

band in the presence and absence of EGF. Total EGFR levels were again significantly ($p < 0.05$) decreased by NDRG1 expression relative to the VC counterparts (Fig. 3*A*). Additionally, EGFR was also slightly decreased by MG132 in both VC and N1 cells in the presence or absence of EGF relative to the respective controls.

When examining pEGFR at Tyr-1068, EGF was able to markedly and significantly ($p < 0.001–0.01$) increase its levels relative to the respective controls without EGF in both VC and N1 cells, as expected. In both VC and N1 cells, MG132 was able to significantly ($p < 0.05$) increase pEGFR (Tyr-1068) levels in the presence of EGF relative to the control incubated with EGF alone (Fig. 3*A*). This was despite the ability of NDRG1 expression to significantly ($p < 0.05$) reduce pEGFR (Tyr-1068) levels relative to the respective VC control treated with MG132 in the presence of EGF (Fig. 3*A*). Additionally, the ratios of pEGFR to EGFR were calculated, with MG132 and EGF treatment significantly ($p < 0.01$) increasing the ratio relative to EGF alone in VC cells, whereas in N1 cells there was an increase ($p > 0.05$) with MG132 and EGF (Fig. 3*A*). Together, these observations suggest that inhibiting proteasomal activity plays a role in preventing the decrease in pEGFR (Tyr-1068) levels in the presence and absence of NDRG1 overexpression.

The effect of lactacystin on NDRG1 expression (Fig. 3*B*) was similar to that observed for MG132 (Fig. 3*A*). lactacystin also had similar effects to MG132 on EGFR (Fig. 3*B*). However, in contrast to MG132, incubation with lactacystin only slightly decreased pEGFR (Tyr-1068) in the presence of EGF in both VC and N1 cells (Fig. 3*B*). Additionally, the ratios of pEGFR to EGFR were calculated, with lactacystin and EGF treatment not significantly ($p > 0.05$) increasing the ratio relative to EGF alone in VC or N1 cells (Fig. 3*B*). As lactacystin has a different proteasomal inhibitory profile to MG132, this may explain the difference observed between these studies.

Of note, it has been shown that polyubiquitination of EGFR by the proteasome is needed to allow for lysosomal sorting of activated EGFR, suggesting the proteasome may, in part, assist trafficking and/or processing of EGFR. Furthermore, similarly to our current studies, MG132 has been demonstrated to increase pEGFR levels in the presence of EGF. Overall, there is some evidence from this investigation and previous studies with MG132 to suggest involvement of proteasomal processing in EGFR trafficking/processing.

Association of MIG6 and NDRG1 as demonstrated by co-immunoprecipitation and confocal microscopy

Taking into account the effects of NDRG1 on inhibiting EGFR expression (see Figs. 1, *A* and *C*, and 2 and 3), and the role of MIG6 in promoting EGFR processing by the lysosome (33), it was important to understand how exactly these proteins affect each other. In these studies, PANC-1 lysates were immunoprecipitated with NDRG1 antibody, and then NDRG1 or MIG6 levels examined by Western blotting (Fig. 3*A*). When NDRG1 was immunoprecipitated and then assessed for NDRG1 expression by Western blotting as a control, significantly higher ($p < 0.05$) levels of NDRG1 were observed in the N1 cells relative to the VC cells in the presence and absence of EGF (Fig. 3*A*). Of note, when using the co-immunoprecipitation protocol, the 46-kDa NDRG1 band was not present or faintly present in either the input (Western only) or the IP for the N1 overexpression clone (Fig. 3*A*). In contrast, for VC cells, the 46-kDa band is present in both the input and the IP. This was a highly consistent finding throughout many experiments. A similar effect was also sometimes observed for the Westerns (*e.g.* Fig. 1, *A* and C), where the 46-kDa band is present in VC cells, but less visible in the N1 clones with high exogenous NDRG1 expression at 48 kDa. Considering this, we speculate that it may be because of three possible reasons: 1) the high expression of the exogenous NDRG1 48-kDa band sometimes overshadows the 46-kDa NDRG1 band, making it less visible; 2) alternatively, there appears to be some association between the two bands in N1 clones, leading to the appearance of the significantly larger 48-kDa NDRG1 band (Fig. 3*A*); and/or 3) the high levels of exogenous NDRG1 somehow influences endogenous 46 kDa NDRG1. Irrespective of the cause in the shift of the 46-kDa band, the higher total NDRG1 expression up-regulates MIG6.

Importantly, the NDRG1 immunoprecipitate was also found to contain substantial MIG6 levels, which was significantly ($p < 0.05$) increased in N1 cells when compared with VC cells regardless of EGF treatment (Fig. 3*A*). These observations suggest a possible association between MIG6 and NDRG1.

To further examine the potential association of NDRG1 with MIG6, co-localization between these proteins was assessed using confocal microscopy (Fig. 3*B*). As this technique images cells on a single lateral focal plane, only molecules in the same location are co-localized (55). In the VC control and EGF-treated samples, MIG6 was mainly distributed in the cytosol as very fine puncta, whereas NDRG1 was present in both the cytosol and nucleus, again as fine puncta, with little co-localization being evident ($r = 0.549 – 0.646$). This distribution agrees with previous studies assessing the subcellular localization of MIG6 (32) and NDRG1 (15, 43).

Upon NDRG1 overexpression in N1 cells, the overall intensity of both NDRG1 and MIG6 markedly and significantly ($p < 0.001$) increased, resulting in intense clustering of MIG6 staining predominantly in the cytosol (Fig. 3*B*). On the other hand, for NDRG1 expression, in the N1 control and EGF-treated cells, its distribution was both cytoplasmic and nuclear. This distribution of NDRG1 and MIG6 upon NDRG1 overexpression in the presence and absence of EGF, led to a marked and significant ($p < 0.001$) increase in co-localization in the cytoplasm ($r = 0.873 – 0.881$), suggesting increased association between these proteins. These results in terms of NDRG1 and MIG6 expression are in agreement with the Western blotting data (Fig. 1*A*), whereas the co-localization is concordant with the co-immunoprecipitation results (Fig. 3*A*). Together, these data in Fig. 3, *A* and *B*, suggest an association of MIG6 and NDRG1 in the cytosol of cells that overexpress NDRG1, and prompted further dissection into the mechanisms involved in NDRG1's attenuation of EGFR signaling mediated via MIG6.

EGFR does not directly associate with NDRG1

Overall, the studies above in Fig. 3 indicate MIG6 and NDRG1 associate to form a potential complex. As an additional confirmation of this observation, PANC-1 lysates were immunoprecipitated with MIG6 antibody, and then MIG6, EGFR, or NDRG1 levels examined by Western blotting (Fig. 4*A*). When MIG6 was immunoprecipitated and then assessed for MIG6 expression by Western blotting as a control, markedly and significantly ($p < 0.001$) higher levels of MIG6 were observed in N1 cells relative to the VC cells in the presence and absence of EGF (Fig. 4*A*). Assessing EGFR levels in the MIG6 immunoprecipi-

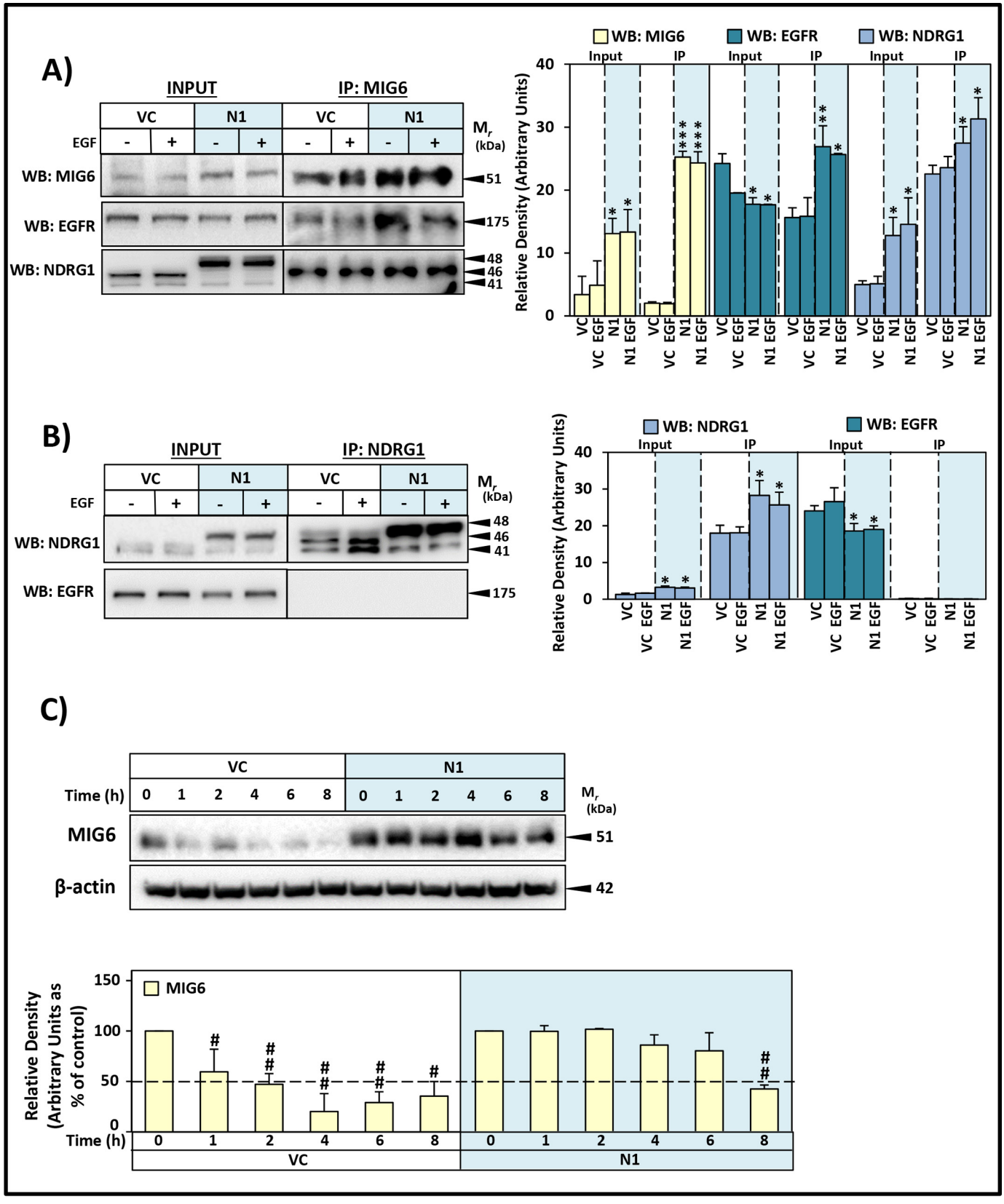

Figure 4. *A–C*, EGFR (*A* and *B*) does not directly associate with NDRG1, but (*C*) NDRG1 overexpression increases the half-life of MIG6. PANC-1 VC or N1 cells were incubated with control media or media containing EGF (10 ng/ml; 10 min/37 °C) and examined via co-immunoprecipitation. MIG6 (*A*) or NDRG1 (*B*) was immunoprecipitated and Western blotting performed to detect MIG6, EGFR, or NDRG1 expression. Input lysates of the total protein were included for comparison with immunoprecipitated lysates for each sample. Relative to untreated vector control cells: *, $p < 0.05$; **, $p < 0.01$ and ***, $p < 0.001$ in the respective condition. *C*, PANC-1 VC and N1 cells were preincubated with cycloheximide (10 μg/ml) for 1 h/37 °C with EGF being added in the last 10 min and the incubation then continued for 1–8 h/37 °C. Results are typical blots from three performed and the densitometry is mean ± S.D. (three experiments). #, $p < 0.05$ and ##, $p < 0.01$ are relative to the 0 h time point.

tate, it was demonstrated to be significantly (p <0.01–0.05) up-regulated in N1 cells, both with and without EGF treatment (Fig. 4*A*), suggesting an association between these proteins, particularly in the presence of NDRG1 overexpression. Further, the MIG6 immunoprecipitate contained substantial NDRG1 levels, which was significantly (p <0.05) increased in N1 cells (Fig. 5*A*). Notably, the MIG6 immunoprecipitate contained predominantly the 46-kDa isoform of NDRG1, which again is consistent with the active form of NDRG1 that has been shown to inhibit metastasis (16, 35, 43). Hence, this was further evidence supporting the MIG6 and NDRG1 interaction observed in Fig. 3*A*.

Because MIG6 is known to directly bind to EGFR (26, 56), it can be hypothesized that NDRG1 may also bind to EGFR. To examine this, PANC-1 lysates were immunoprecipitated with NDRG1 antibody and NDRG1 and EGFR levels then examined by Western blotting (Fig. 4*B*). When NDRG1 was pulled down, EGFR was not present in the immunoprecipitate. This was despite the fact that the procedure was successful in immunoprecipitating MIG6 and also NDRG1 itself (Fig. 3*A*). Furthermore, immunoprecipitation with the EGFR antibody also resulted in no detection of NDRG1 (Fig. S4*B*). Collectively, these results in Figs. 3, *A* and *B*, and 4, *A* and *B*, and Fig. S4*B* suggest that NDRG1 directly associates with MIG6, but not EGFR.

To further examine any possible association of NDRG1 with EGFR, co-localization between these proteins was assessed using confocal microscopy (Fig. S3). Again, EGFR expression was significantly (p <0.001–0.01) decreased by NDRG1 expression in N1 cells (Fig. S3*i*). However, little co-localization was evident between NDRG1 and EGFR (r = 0.428–0.487). Unlike the studies examining MIG6 and NDRG1 association (Fig. 3*B*), quantification of co-localization demonstrated no significant increase in the merged images in N1 cells relative to VC cells (Fig. S3*ii*).

Collectively, these studies in Fig. S3 suggest that there was no marked association between NDRG1 and EGFR. Considering this and the results in Figs. 3 and 4*B*, it can be hypothesized that NDRG1 may stabilize MIG6 to increase its half-life. Thus, as a theoretical model, the increased half-life of MIG6 would enable its binding to EGFR, with NDRG1 then dissociating, resulting in its not being detected with the EGFR.

NDRG1 overexpression increases MIG6 protein half-life

To assess the hypothesis that NDRG1 stabilizes MIG6 to increase its half-life, PANC-1 VC and N1 cells were preincubated with cycloheximide (10 μg/ml) for 1 h/37 °C, with EGF being added in the last 10 min and the incubation then being continued for 1–8 h/37 °C, as per standard protein stability assessment protocols (57, 58). From Fig. 4*C*, Western blotting demonstrated the half-life of MIG6 in VC cells was calculated as 1.6 ± 0.2 h (3), which was very similar to previous reports using another cell type (*i.e.* 90–120 min) (59). Interestingly, compared with VC cells, the half-life of MIG6 was significantly (p <0.001) increased to 7.9 ± 0.4 h (3), which could explain 1) the significantly higher levels of MIG6 in N1 cells, 2) the post-transcriptional regulation of MIG6 (Fig. S1*D*), and 3) the ability of MIG6 to more markedly down-regulate EGFR expression in N1 relative to VC cells.

MIG6 is involved in the NDRG1-mediated down-regulation of EGFR

We have demonstrated previously (21) and herein (Figs. 1–3), that NDRG1 is able to down-regulate EGFR. Further, in this investigation, we have shown that NDRG1 up-regulates MIG6 protein levels (Figs. 1*A* and 3*B*), and intriguingly there is an association between NDRG1 and MIG6, but not NDRG1 and EGFR (Figs. 3 and 4 and Fig. S3). To dissect the potential role of MIG6 in the ability of NDRG1 to down-regulate EGFR, PANC-1 cells were transiently transfected with *MIG6* siRNA (siMIG6) or nonspecific control siRNA (siControl). Then MIG6, EGFR, pEGFR (Tyr-1068), and NDRG1 levels were examined in the presence and absence of EGF by Western blotting (Fig. 5*A*).

In these studies, effective silencing of *MIG6* was achieved, with a significant (p <0.01) decrease of MIG6 levels in VC and N1 cells. Additionally, similar to Fig. 1*A*, MIG6 was significantly (p <0.05) increased in N1 compared with VC siControl cells. When examining EGFR levels, NDRG1 expression in N1 cells resulted in a significant (p <0.01–0.05) decrease in its levels, in the presence and absence of EGF. Interestingly, a slight, but significant increase (p <0.05) of EGFR was observed in VC cells when MIG6 was silenced (siMIG6) in the presence and absence of EGF (Fig. 5*A*). Notably, the effect of siMIG6 was markedly more pronounced at significantly (p <0.05) increasing EGFR levels in N1 cells, irrespective of EGF treatment when compared with siControl N1 cells. This finding demonstrates the importance of MIG6 in the NDRG1-mediated decrease of EGFR expression.

Assessing pEGFR (Tyr-1068), its levels were also significantly (p <0.05) enhanced upon MIG6 silencing in both VC and N1 cells (Fig. 5*A*). However, this effect was less marked in N1 cells, with NDRG1 overexpression markedly decreasing the overall pEGFR levels relative to VC cells. This latter finding suggests the NDRG1-mediated decrease of pEGFR (Tyr-1068) is occurring, at least in part, via MIG6.

Silencing PTEN decreases MIG6 and results in up-regulation of total EGFR and increased pEGFR (Tyr-1068) levels in the presence and absence of NDRG1 overexpression

Previous studies have shown that the tumor suppressor PTEN is able to attenuate EGFR signaling by promoting the maturation of early to late endosomes (60). To decipher the involvement of PTEN in the ability of NDRG1 to down-regulate EGFR via MIG6, PANC-1 cells were transiently transfected with *PTEN* siRNA (siPTEN) or nonspecific control siRNA (siControl), and PTEN, EGFR, pEGFR (Tyr-1068), MIG6, and NDRG1 levels were examined in the presence and absence of EGF (Fig. 5*B*).

Efficient down-regulation of PTEN expression was achieved by siPTEN, with a significant (p <0.01) decrease of PTEN levels in both VC and N1 cells. When assessing EGFR levels, NDRG1 expression in N1 cells again significantly (p <0.01–0.05) decreased EGFR in the siControl treatment group. However, in

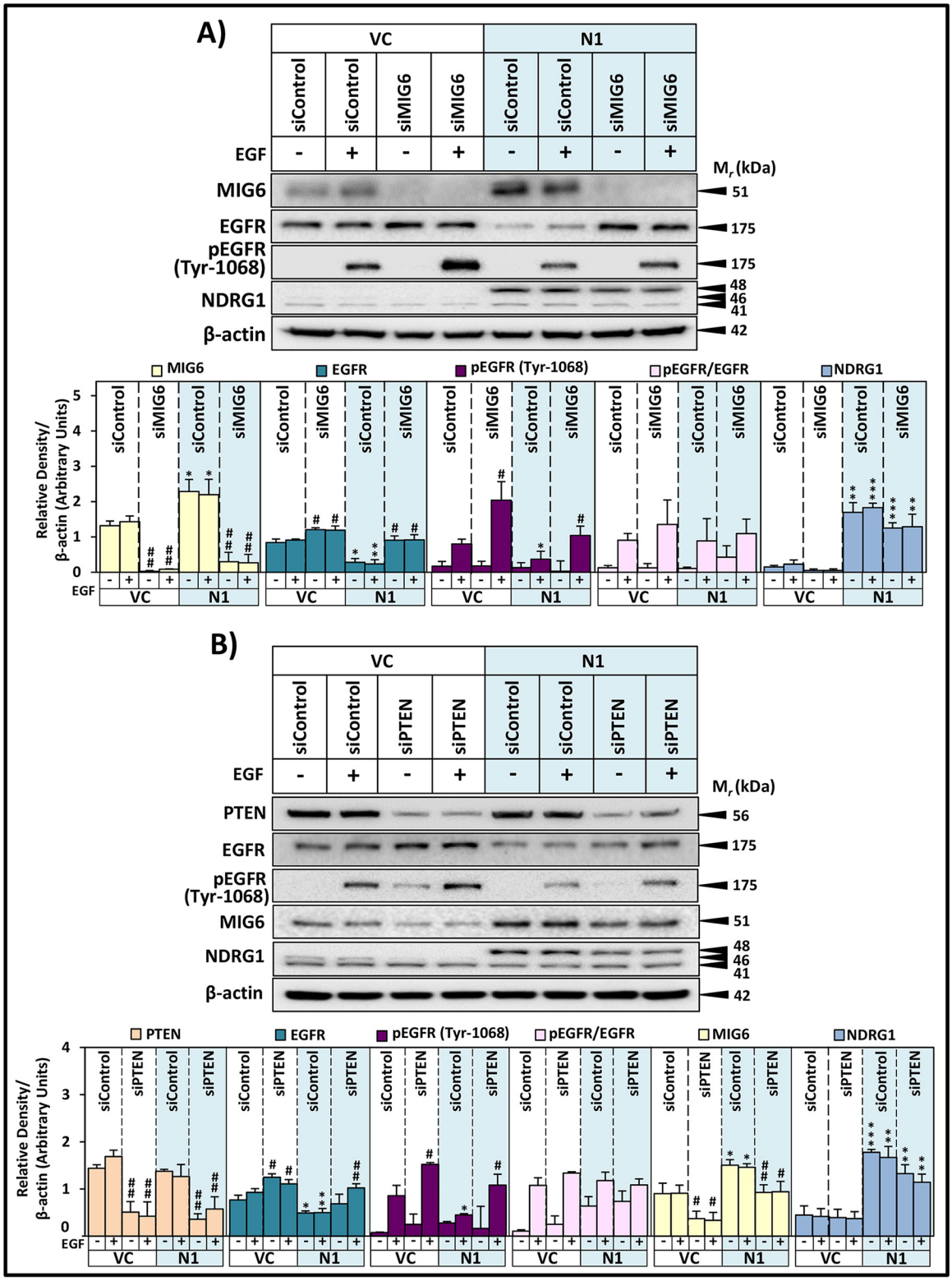

Figure 5. Silencing of the tumor suppressors *MIG6* and *PTEN* increases total and activated EGFR levels. *A* and *B*, PANC-1 VC or N1 cells were transiently transfected with nonspecific control siRNA (siControl) and (*A*) *MIG6* siRNA (siMIG6) or (*B*) *PTEN* siRNA (siPTEN), followed by incubation with control media or this media containing EGF (10 ng/ml; 10 min/37 °C). Total cell protein was extracted and electrophoresed on a 10% SDS-PAGE gel followed by Western blot analysis to detect MIG6, NDRG1, EGFR, pEGFR (Tyr-1068), or PTEN expression. β-actin was used as a protein-loading control. Results are mean ± S.D. ($n = 3$). *, $p < 0.05$; **, $p < 0.01$; ***, $p < 0.01$ denote statistical significance comparing NDRG1 overexpressing cells relative to VC cells. #, $p < 0.05$; ##, $p < 0.01$ denotes statistical significance comparing siRNA-treated cells to their respective siControl within VC or N1 cells.

VC cells, siPTEN caused a slight and significant ($p < 0.05$) increase of EGFR in the presence and absence EGF (Fig. 5*B*).

Similarly, siPTEN also slightly, but significantly ($p < 0.01$) increased EGFR in N1 cells, but only with EGF-treatment. This is consistent with the role of PTEN in enhancing EGFR degradation (60) and siPTEN decreasing this. Examining pEGFR (Tyr-1068) levels, siPTEN resulted in a significant ($p < 0.05$) 2.0- to 2.1-fold increase in its levels only in the presence of EGF in both VC and N1 cells (Fig. 5*B*). Although siPTEN caused a similar -fold increase in both VC and N1 cells, the overall levels of pEGFR (Tyr-1068) were markedly and significantly ($p < 0.05$) decreased with NDRG1 expression in N1 cells. Together, these findings suggest PTEN is also involved, at least in part, in the NDRG1-mediated degradation of EGFR.

Of interest, siPTEN resulted in a significant ($p < 0.01–0.05$) decrease in MIG6 expression in both VC and N1 cells relative to their respective siControls in the presence and absence of EGF (Fig. 5*B*). This result indicates that the ability of PTEN to facilitate the down-regulation of EGFR (60) could be mediated through the up-regulation of MIG6. Collectively, these results suggest a role for PTEN in regulating MIG6.

The novel thiosemicarbazones Dp44mT and DpC up-regulate NDRG1 and MIG6 and promote their co-localization

As shown herein, NDRG1 is able to promote the degradation of a master regulator of oncogenic signaling, EGFR, via the up-regulation of MIG6. Given the demonstrated ability of NDRG1 to suppress metastasis, this makes it a viable therapeutic target for cancer therapy (10). NDRG1 is potently up-regulated by the novel DpT class of anti-cancer agents that includes Dp44mT and DpC (10, 35) (Fig. S1*A*), the latter of which has entered clinical trials (40). In this study, the two lead agents, Dp44mT and DpC, were used in addition to the positive control, DFO (Fig. S1*A*), which is a well-known iron chelator used to treat iron overload disease (61). A negative control, 2-benzoylpyridine 2-methyl-3-thiosemicarbazone (Bp2mT), was also used, as it is an analog of Dp44mT and DpC, which was specifically designed not to bind metal ions or show anti-tumor activity (62). Although the lipophilic and permeable Bp2mT, Dp44mT, and DpC (10, 35) were examined at 10 μM, DFO was used at 250 μM, because of its greater hydrophilicity, which leads to poor membrane permeabilization (34, 63).

As demonstrated in previous studies (10, 35), DFO, Dp44mT, and DpC were all able to markedly and significantly ($p < 0.001$) up-regulate NDRG1 in PANC-1 cells (Fig. 6*A*). Both Dp44mT and DpC also significantly ($p < 0.001–0.01$) decreased EGFR expression. Additionally, DpC significantly ($p < 0.05$) decreased pEGFR (Tyr-1068), whereas Dp44mT was not as effective ($p > 0.05$) in reducing its levels (Fig. 6*A*). As we observed previously (21), the pEGFR (Tyr-1068)/total EGFR was not significantly altered relative to the control by these agents, suggesting the decrease in total EGFR resulted in reduction in its phosphorylated levels. These agents also potently and significantly ($p < 0.001–0.05$) increased HIF-1α expression, which is important, as this transcription factor targets MIG6 (42).

In good agreement with the increased HIF-1α levels, MIG6 was also markedly and significantly ($p < 0.001–0.01$) up-regulated by these agents, with DFO being less effective than either Dp44mT or DpC (Fig. 6*A*). Collectively, these agents up-regulate MIG6 probably via HIF-1α that induces NDRG1 expression (10), which then decreases EGFR expression and activation. This is notable, as MIG6 has been demonstrated to suppress tumor formation (64), and its ability to be harnessed by a therapeutic agent has not been investigated previously.

To further investigate these promising results, the effect of our novel agents was then assessed using confocal microscopy to examine the intracellular distribution and co-localization of MIG6 and NDRG1 in PANC-1 cells incubated for 24 h/37 °C with our agents (Fig. 6*B*), under the conditions described above in Fig. 6*A*. The expression of MIG6 was predominantly cytoplasmic, whereas NDRG1 was both cytoplasmic and nuclear. The levels of MIG6 and NDRG1 were significantly ($p < 0.01–0.001$) increased after incubation with DFO, and especially Dp44mT and DpC (Fig. 6*Bi*). This result was in good agreement with the Western blotting data (Fig. 6*A*). Quantification analysis demonstrated significantly ($p < 0.001$) increased co-localization of MIG6 and NDRG1 (*i.e.* yellow fluorescence) in cytoplasmic puncta particularly after incubation with Dp44mT and DpC, which was accompanied by an increase in the Pearson's correlation coefficient from $r = 0.516$ in the control to $r = 0.814–0.913$ (Fig. 6*Bii*). It is of interest to note that DFO demonstrated less efficacy than both Dp44mT and DpC at increasing MIG6 expression (Fig. 6*A*), which led to less co-localization with NDRG1 (Fig. 6*B*). This decreased efficacy of DFO is probably related to its greater hydrophilicity and poorer membrane permeability relative to the lipophilic and highly membrane-permeable Dp44mT and DpC (34, 36). Together, these data in Fig. 6 indicate that the anti-cancer agents Dp44mT and DpC markedly up-regulate NDRG1 and MIG6, which co-localize intracellularly.

To demonstrate the mechanism by which the thiosemicarbazones up-regulate MIG6, in Fig. S4*A* we have examined the effect of the agents used in Fig. 6, *A* and *B*, on MIG6 expression upon NDRG1 silencing after a 24-h/37 °C incubation. In siControl cells, Dp44mT and DpC robustly increased MIG6 expression. In contrast, after NDRG1 silencing, both agents were markedly less effective at up-regulating MIG6 (Fig. S4*A*). These results indicate that the up-regulation of MIG6 by Dp44mT and DpC depends on NDRG1 expression.

DpC and Dp44mT promote EGFR and LAMP2 co-localization

Next, considering the results in Fig. 6 above regarding the up-regulation of MIG6 and its co-localization in intracellular vesicles by our agents, studies then assessed if this could result in degradation of EGFR via the induction of lysosomal processing (33). Hence, studies examined the effect of these agents on inducing EGFR redistribution and co-localization with LAMP2-stained late endosomes/lysosomes using confocal microscopy (Fig. 7). In control and Bp2mT- and DFO-treated PANC-1 cells, EGFR (*red*) showed distinct plasma membrane staining with some fine punctate cytosolic staining, whereas the LAMP2 late endosome/lysosomal marker (*green*) was finely distributed in puncta within the cytosol. Upon quantification,

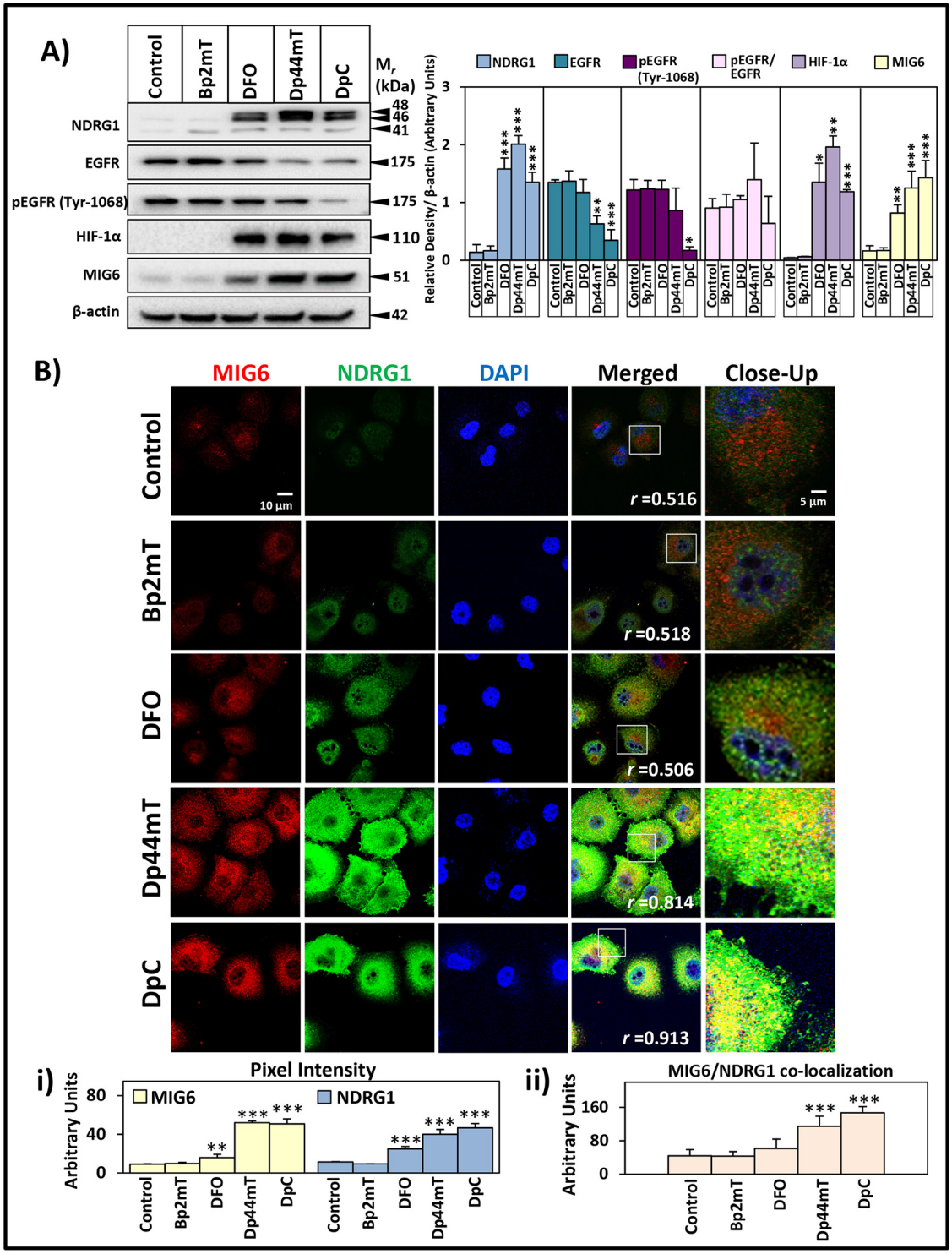

Figure 6. *A* and *B*, the thiosemicarbazones Dp44mT and DpC up-regulate MIG6 expression (*A*) and increase co-localization (*B*) between MIG6 and NDRG1. PANC-1 cells were incubated with either control medium or medium containing Bp2mT (10 μM), DFO (250 μM), Dp44mT (10 μM), or DpC (10 μM) in the presence of EGF (10 ng/ml) for 24 h/37 °C. *A*, total cell protein was extracted and electrophoresed on a 10% SDS-PAGE gel followed by Western blot analysis to detect NDRG1, EGFR, pEGFR (Tyr-1068), HIF-1α, and MIG6 expression. β-actin was used as a protein-loading control. Results are mean ± S.D. ($n = 3$). *, $p < 0.05$; **, $p < 0.01$; ***, $p < 0.001$ denote comparison to control cells. *B*, confocal immunofluorescence images show staining for MIG6 (*red*), NDRG1 (*green*), and DAPI for nuclei (*blue*). All images were taken with a 63× objective and at the same exposure time using AxioVision™ software. Quantification of (*Bi*) MIG6 and NDRG1 pixel intensity and (*Bii*) MIG6/NDRG1 co-localization were performed using ImageJ software and these results are mean ± S.D. (three experiments). **, $p < 0.01$ and ***, $p < 0.001$ are relative to the control. Pixel intensity and co-localization analysis utilized a total of 30–40 cells over three experiments. *B*, the *scale bar* in the *bottom right-hand corner* of the first image represents 10 μm and is the same across all images, except the *close-up panel*, where the *scale bar* is 5 μm.

only limited co-localization ($r = 0.228 – 0.426$) of the EGFR and LAMP2 marker was detected in control and Bp2mT- and DFO-treated cells (Fig. 7*ii*).

In contrast, treatment of PANC-1 cells with Dp44mT and DpC resulted in pronounced clustering of EGFR intracellularly into defined foci. Similarly, LAMP2 staining was also markedly

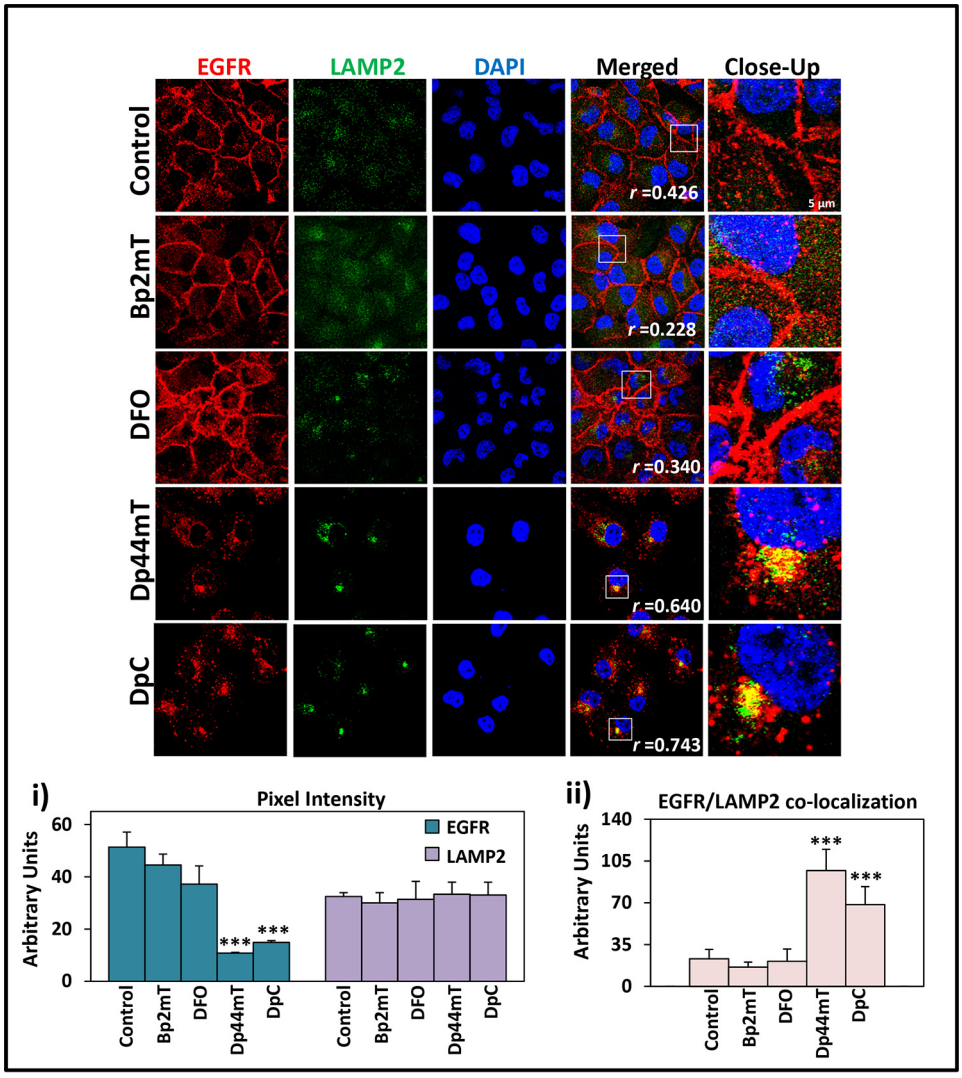

Figure 7. Incubation of cells with Dp44mT and DpC decreases EGFR expression and increases EGFR co-localization with the late endosome/lysosomal marker LAMP2. VC PANC-1 cells were incubated with either control medium or medium containing Bp2mT (10 μM), DFO (250 μM), Dp44mT (10 μM), or DpC (10 μM) in the presence of EGF (10 ng/ml) for 24 h/37 °C. Immunofluorescence images show staining for EGFR (*red*), LAMP2 (*green*), and DAPI for nuclei (*blue*). All images were taken with a 63× objective and at the same exposure time using AxioVision™ software. Images are representative from three experiments performed. Quantification of (*i*) EGFR and LAMP2 pixel intensity and (*ii*) EGFR/LAMP2 co-localization were performed using ImageJ software and are mean ± S.D. (three experiments). ***, $p < 0.001$ relative to the control. Pixel intensity and co-localization analysis utilized a total of 30–60 cells over three experiments. The *scale bar* in the *bottom right-hand corner* of the first image represents 10 μm and is the same across all images, except the *close-up panel*, where the *scale bar* is 5 μm.

altered upon treatment with DpC and Dp44mT, resulting in clustering into perinuclear foci that co-localized with EGFR. However, this redistribution of LAMP did not alter its total levels between conditions, with no significant change in pixel intensity being observed (Fig. 7*i*). Notably, there was a significant ($p < 0.001$) increase in the co-localization intensity of EGFR and LAMP2 upon quantification, with a marked increase in Pearson's correlation coefficient from $r = 0.426$ in the control to $r = 0.640–0.743$ in Dp44mT- and DpC-treated cells (Fig. 7). Once again, the efficacy of DFO at reducing EGFR was less marked than that found for Dp44mT and DpC, probably because of its lower membrane permeability (34, 36, 63). This resulted in decreased induction of MIG6 expression by DFO relative to Dp44mT and DpC (Fig. 6, *A* and *B*), and thus, no significant effect on reducing EGFR expression (Figs. 6*A* and 7). Collectively, these studies in Fig. 7 demonstrate that the novel anti-cancer agents Dp44mT and DpC up-regulate MIG6 and promote EGFR localization to LAMP2-defined late endosomes/lysosomes.

Discussion

Metastasis is the major killer in cancer (65), which remains the "emperor of all maladies." Understanding the mechanisms of action of metastasis suppressor proteins that block metastasis could lead to new therapeutic targets. The metastasis suppressor NDRG1 has demonstrated comprehensive anti-cancer activity via its ability to inhibit a series of critical oncogenic signaling pathways that play roles in metastasis and cancer progression (12, 13, 15, 16, 18). As such, a major question in the field was how does NDRG1 inhibit the activity of such a broad range of signaling pathways? Recently, our laboratory has reported that NDRG1 could effectively do this via its ability to down-regulate a master regulator of these pathways, namely

EGFR (20, 21). In fact, these studies indicated that NDRG1 expression accelerated the loss of EGFR monomers and dimers relative to control cells in the presence of EGF, suggesting that NDRG1 facilitated its processing (21). The current study investigated the mechanisms involved in this effect.

The degradation of EGFR is largely controlled by MIG6 (33), which is a cytoplasmic protein (32) that down-regulates EGFR activity by direct inhibition of the EGFR dimer (26) and induces lysosomal processing (33). We demonstrate that NDRG1 expression markedly increased MIG6 levels, whereas silencing *NDRG1* in multiple cell types decreased MIG6, demonstrating that NDRG1 is able to regulate this protein. Notably, there is no evidence in the literature that NDRG1 induces its effects by acting as a transcription factor, and the up-regulation of MIG6 observed herein was not because of an increase in *MIG6* mRNA levels after up-regulation of NDRG1, suggesting a posttranscriptional mechanism of regulation. Indeed, we demonstrate that NDRG1 markedly extends the protein half-life of MIG6, suggesting that it functions to stabilize this molecule. An important finding was that MIG6 became bound to NDRG1, but not EGFR, in the cytoplasm, as determined using both co-immunoprecipitation and co-localization using confocal microscopy. This direct interaction may be key to how NDRG1 enhances the half-life of MIG6.

The well-characterized lysosomotropic agents NH_4Cl and CH_3NH_2 that inhibit endosomal and lysosomal acidification (48, 66, 67) were demonstrated to reverse the effects of NDRG1 on decreasing pEGFR (Tyr-1068) and increasing MIG6, suggesting perturbation of the acidic lysosomal pH interferes with EGFR and MIG6 processing. The increased MIG6 levels increased EGFR internalization and co-localization of EGFR with the early endosome marker, EEA1, and the late endosome/lysosome marker, LAMP2.

From these results, a model of the interaction between these molecules can be proposed, whereby NDRG1 increases MIG6 expression by a posttranscriptional mechanism, potentially by binding to it and stabilizing its protein levels. As such, NDRG1 may also facilitate MIG6 binding to EGFR, resulting in its inhibition and the late endosomal/lysosomal processing of EGFR (Fig. 8). As discussed above, relative to the strong co-localization between LAMP2 and EGFR, no appreciable co-localization was observed between LAMP2 and NDRG1, or LAMP2 and MIG6. This suggests that the effect of NDRG1 and MIG6 on increasing EGFR processing via the lysosome could occur prior to its internalization into the lysosomal compartment (Fig. 8).

Supporting evidence for this model comes from studies where *MIG6* silencing reversed the inhibitory effect of NDRG1 on EGFR expression (Fig. 5*A*), suggesting a role for MIG6 in the NDRG1-mediated down-regulation of the EGFR. Importantly, the direct binding of MIG6 to EGFR was also significantly increased in NDRG1 overexpressing cells, further demonstrating that NDRG1 is enhancing the formation of the MIG6–EGFR complex. Silencing *PTEN,* which is known to augment early to late endosome maturation (60), decreased MIG6 in the presence and absence of NDRG1 overexpression, with a concurrent increase in EGFR and pEGFR (Tyr-1068) levels. Hence, the PTEN-mediated trafficking of endosomes to lysosomes (60) may play a role in MIG6-directed processing of EGFR and pEGFR.

Of note, *NDRG1* silencing in epithelial cells was previously reported to decrease the uptake of low-density lipoprotein (68), which suggests a potential shared, and more general, role for this metastasis suppressor in receptor internalization and vesicular trafficking. However, the direct interaction of NDRG1 with MIG6 and the formation of an MIG6–NDRG1 complex probably accounts for the increased levels and stability of MIG6 (Fig. 4*C*), which facilitates EGFR processing by the lysosome.

Unlike most metastasis suppressors that are yet to be targeted by pharmacological interventions, it has been demonstrated that novel anti-cancer agents of the DpT class, namely Dp44mT and DpC (22, 34, 36), can up-regulate NDRG1 expression (10, 35). This effect of these agents is known to occur through both HIF-1α– dependent and –independent processes (10). The mechanism of this induction of NDRG1 is mediated by the pronounced iron chelation efficacy of Dp44mT and DpC (34, 36), which inhibits the activity of prolyl hydroxylase that requires iron in its active site and is critical for HIF-1α degradation (69). The inhibition of prolyl hydroxylase results in increased HIF-1α levels (Fig. 6*A*) that then lead to increased transcription of its downstream targets, which include *NDRG1* (10). This effect of HIF-1α could be responsible for the marked up-regulation of MIG6 observed after incubation of cells with DpC and Dp44mT (Fig. 6*A*), as MIG6 is a known transcriptional target of HIF-1α (42). Relevant to this, the up-regulation of MIG6 was demonstrated after incubation of cancer cells with several well-characterized iron chelators (41). Furthermore, the concurrent up-regulation of both NDRG1 and MIG6 via HIF-1α could then lead to stabilization of MIG6 through its binding to NDRG1, as shown herein. In fact, silencing of NDRG1 prevented the ability of Dp44mT and DpC to markedly up-regulate the EGFR inhibitor MIG6. Hence, the potent effects of Dp44mT and DpC are, at least in part, because of the up-regulation of NDRG1 and its effects on increasing MIG6 levels.

Importantly, the effect of these pharmacological agents on up-regulating both NDRG1 and MIG6 expression was very similar to that observed by genetic overexpression of NDRG1, with the following being observed: NDRG1 co-localization being demonstrated with MIG6 in the cytosol (*cf.* Figs. 3*B* and 6*B*), decreased total and activated EGFR levels (*cf.* Figs. 1*A* and 7), and redistribution of EGFR to LAMP2-stained late endosomes/lysosomes (*cf.* Figs. 2*B* and 7). Moreover, both Dp44mT and DpC also markedly inhibit PANC-1 pancreatic tumor xenograft growth *in vivo*, demonstrating their potent activity (10, 35). In fact, DpC was demonstrated to show greater activity than a "gold standard" agent for pancreatic cancer treatment, namely gemcitabine, with DpC totally inhibiting PANC-1 tumor xenograft growth (10, 35).

In conclusion, the clinical trial DpT group of agents can down-regulate a "master switch" of oncogenic signaling, namely EGFR, via an entirely different molecular mechanism currently employed to target this tyrosine kinase. That is, by up-regulating NDRG1 to increase MIG6 expression via enhancing its half-life. As such, the DpT compounds provide an innovative strategy for treating cancer, with these agents being capable of 1) potently inhibiting the growth and metastasis *in*

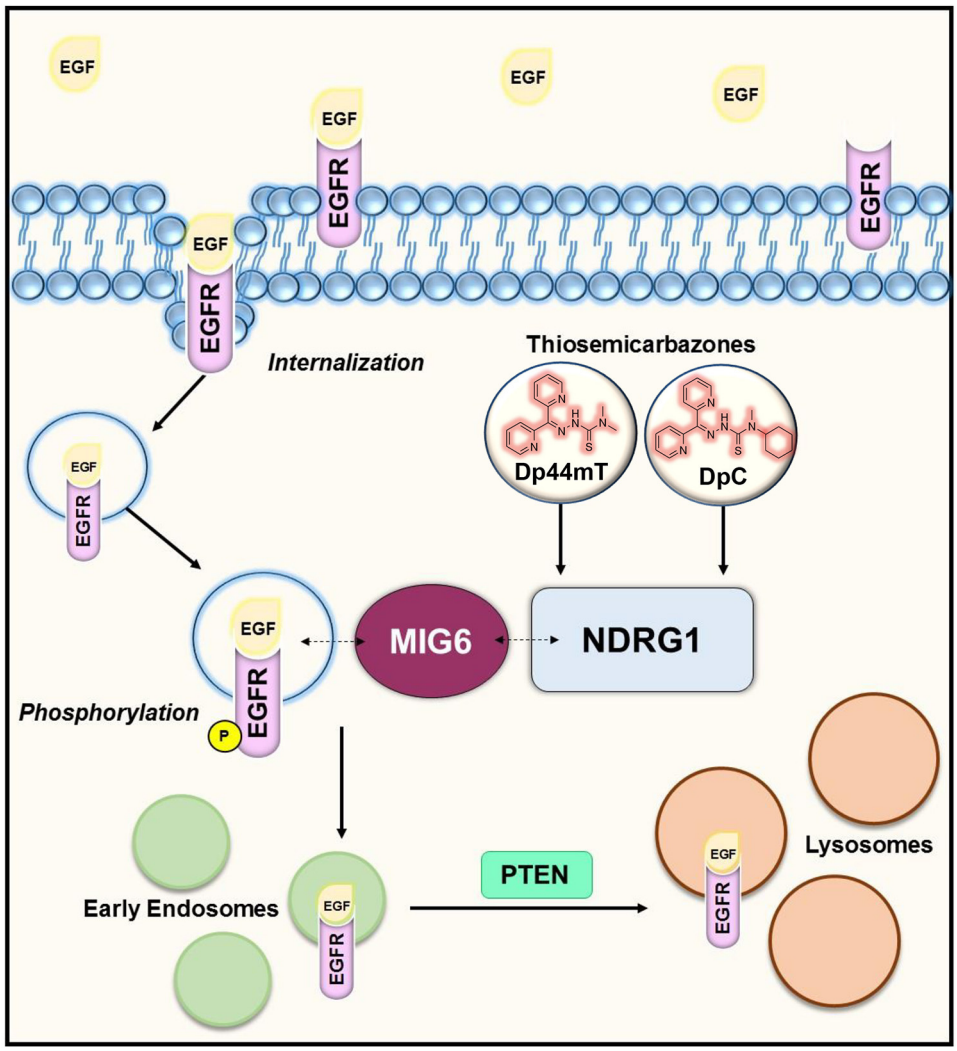

Figure 8. Schematic illustrating the role of NDRG1 and MIG6 in facilitating EGFR processing by the lysosomal compartment. EGF binds to EGFR, inducing its internalization via endocytosis into the cell leading to EGFR in early endosomes and lysosomes. The tumor suppressor PTEN has been demonstrated to play a role in the trafficking of early endosomes to lysosomes (60). The novel di-2-pyridylketone thiosemicarbazones Dp44mT and DpC bind and deplete cellular iron (10, 34, 35), which inhibits prolyl hydroxylase activity and results in up-regulation of NDRG1 via HIF-1α–dependent and –independent mechanisms (10). Depletion of cellular iron also up-regulates MIG6 potentially via HIF-1α (41). Subsequently, MIG6 down-regulates EGFR by directly binding to it and inhibiting the EGFR dimer (26) and inducing EGFR internalization and processing by the lysosome (33). Notably, MIG6 binds to NDRG1 in the cytosol, with increased stabilization of MIG6 being observed in NDRG1 overexpressing cells. This increased half-life of MIG6 probably increases the access of MIG6 to EGFR to ensure down-regulation. However, NDRG1 does not bind to EGFR, with no association of MIG6 or NDRG1 being demonstrated with the late endosome/lysosomal marker, LAMP2. In contrast, NDRG1 expression increases the co-localization of EGFR with EEA1 and LAMP2. In summary, NDRG1 overexpression increases expression of the EGFR inhibitor MIG6 by stabilizing it, resulting in an MIG6-NDRG1 complex that potentiates EGFR down-regulation by enhanced lysosomal processing of EGFR.

vivo of a variety of aggressive cancers (16, 21, 22, 34–38, 70) and 2) markedly inhibiting multiple oncogenic signaling pathways (12–15, 21, 30, 71–73).

Materials and methods

Cell culture

Human pancreatic cancer cell types, namely PANC-1, CFPAC-1, and AsPC-1, were purchased from the American Type Culture Collection (Manassas, VA). These cell types were authenticated based on viability, recovery, growth, morphology, and also cytogenetic analysis, antigen expression, DNA profile, and iso-enzymology by the provider. The cells were maintained in DMEM with 10% fetal calf serum (Life Technologies) and cultured by standard procedures (14) for less than 3 months after resuscitation. Two PANC-1 clones stably transfected to overexpress NDRG1 (N1 and N2) were compared with PANC1 cells transfected with the empty vector (VC), as described previously (12, 14).

siRNA

Two specific siRNAs for *NDRG1* were used, namely siNDRG1 (Cat. # s20336; Life Technologies) and siNDRG1II (Cat. # s20334; Life Technologies), and also an siRNA against *MIG6* (siMIG6; Cat. # AM16708; Ambion), and these were compared with nontargeting negative control siRNA (siControl; Life Technologies). The siRNA was transiently transfected into PANC-1 cells using Lipofectamine 2000 (Life Technologies) and incubated for 72 h/37 °C. Western blotting was then performed. We demonstrated a high positive correlation (r^2 = 0.82–0.83) between NDRG1 down-regulation via siNDRG1 and the decrease in MIG6 expression in all three cell types used (*i.e.* PANC-1, CFPAC-1, AsPC-1) (data not shown). This dem-

onstrates that there is a dose escalation effect between NDRG1 and MIG6 expression. The siRNA specific for *PTEN* (siPTEN) was also compared with siControl but was transiently transfected using RNAiMax (Life Technologies) and incubated for 72 h/37 °C.

Cell treatments

EGF (Cat. # 8916; Cell Signaling Technology, Danvers, MA) was used at 10 ng/ml diluted in 1% FCS-containing media and incubated with cells for 10 min/37 °C. This concentration and time point was implemented based on preliminary studies examining the efficacy of EGF *in vitro* and following that used by previous studies (21, 74). Prior to treatment with EGF, cells were serum-starved in media containing 1% FCS for 24 h/37 °C (75). DFO (Fig. S1*A*) was purchased from Sigma-Aldrich. The thiosemicarbazones Dp44mT and DpC and the negative control compound Bp2mT were synthesized and characterized using standard methods (36, 62, 76). We utilized concentrations of 10 μM for Dp44mT, DpC, and Bp2mT and 250 μM for DFO in 10% FBS-supplemented medium. The greater concentration of DFO was implemented because of its limited ability to permeate the cell membrane (63). Both Dp44mT and DpC were utilized at lower concentrations because these agents show far higher membrane permeability and demonstrate marked iron chelation efficacy (34–36). Bp2mT, Dp44mT, and DpC were freshly dissolved in dimethyl sulfoxide (DMSO) and diluted in culture media (final [DMSO] $\leq$ 0.1%).

Protein extraction and Western blotting

Total protein was extracted using standard procedures in our laboratory (14). Western blot analysis was performed as described previously (77). The primary antibodies used were against human NDRG1 (1:2000 dilution) (Cat. # ab37897; Abcam Inc., Cambridge, MA), EGFR (Cat. # 2085), pEGFR (Tyr-1068) (Cat. # 3777), PTEN (Cat. # 9188), MIG6 (Cat. # 2440), HIF-1α (1:1000 dilution) (Cat. # ab82832; Abcam); β-actin (1:10,000 dilution) (Sigma-Aldrich). The secondary antibodies implemented were anti-goat, anti-rabbit, and anti-mouse (Sigma-Aldrich), each at a dilution of 1:10,000. All antibody dilutions were performed according to the manufacturer's instructions. EGFR, pEGFR(Tyr-1068), PTEN, and MIG6 antibodies were all from Cell Signaling.

Immunofluorescence and confocal microscopy

Immunofluorescence was performed as described (14). Images were captured using a Zeiss LSM 510 Meta Spectral Confocal Microscope (63×) (Zeiss, Jena, Germany). Raw images were analyzed using AxioVision software (Carl Zeiss, Australia). The primary antibodies used were EEA1 (Cat. # ab2900; Abcam), LAMP2 (Cat. # 25631), NDRG1 (Cat. # WH0010397M3; Sigma-Aldrich), and MIG6 (Cat. # PA660708; Thermo Fisher Scientific).

Co-immunoprecipitation

Co-immunoprecipitation was performed using Dynabeads Protein G (Life Technologies) following the manufacturer's instructions. Briefly, cells were washed with ice-cold PBS and lysed using the IP Lysis Buffer (Pierce) containing protease inhibitors (Roche Diagnostics). Protein (400 μg) was incubated with either monoclonal NDRG1 antibody (1:2000 dilution) (Cat. # ab37897; Abcam), EGFR antibody (Cat. # 2085; Cell Signaling Technology), or MIG6 antibody (Cat. # 2440; Cell Signaling Technology) overnight at 4 °C. This mixture was added to 30 μl of Dynabeads Protein G and incubated for 3 h at 4 °C. The beads were then washed three times with ice-cold PBS, and the protein was eluted using the LDS Loading Buffer. Samples were then heated at 95 °C for 5 min and placed on a magnet, and equal amounts of supernatant were loaded and separated on a 10% SDS-PAGE gel. Then NDRG1, MIG6, or EGFR were detected by Western blotting. Notably, control IP experiments using an IgG isotype control antibody (Cat. # 3900; Cell Signaling Technology) were performed under the same conditions. No pull-down was observed when lysates were incubated with the IgG control antibody (Fig. S5). This demonstrates that there was no nonspecific binding to the antibody.

RT-PCR and mRNA analysis

mRNA was isolated using TRIzol® (Thermo Fisher) and semi-quantitative RT-PCR performed using primers for NDRG1 (forward, 5′-GGATCAGTTGGCTGAAAT-3′; reverse, 5′-ATCTTGAGTAGGGTGGTCTT-3′) (size: 513 bp), MIG6 (forward, 5′-AGGCACAATGTCAATAGC A-3′; reverse, 5′-AATCTTCGGTGGGTCTG-3′) (size: 550 bp), EGFR (forward, 5′-TGGAGGGTGAGCCAAGGG-3′; reverse, 5′-CCAGCAGCAAGAGGAGGG-3′) (size: 404 bp), and β-actin (forward, 5′-CCCGCCGCCAGCTCACCATGG-3′; reverse, 5′-AAGGTCTCAAACATGATCTGGGTC-3′) (size: 397 bp) by standard procedures (78). RT-PCR was semi-quantitative, as demonstrated by an optimization protocol showing it was in the log-phase of amplification. β-actin was used as a loading control.

Densitometry

Densitometry was performed using Quantity One software (Bio-Rad) and normalized using the relative β-actin loading control for protein.

Statistics

Data are mean ± S.D. (number of experiments) and were compared using Student's *t* test. Results were considered significant when $p < 0.05$.

Author contributions—S. V. M., Z. K., and D. R. R. conceptualization; S. V. M., Z. K., and D. R. R. data curation; S. V. M., Z. K., and D. R. R. formal analysis; S. V. M., Z. K., and D. R. R. validation; S. V. M., Z. K., and D. R. R. investigation; S. V. M., Z. K., and D. R. R. visualization; S. V. M., Z. K., and D. R. R. methodology; S. V. M., Z. K., and D. R. R. writing-original draft; S. V. M., Z. K., and D. R. R. writing-review and editing; Z. K. and D. R. R. supervision; Z. K. and D. R. R. funding acquisition; Z. K. and D. R. R. project administration; D. R. R. resources; D. R. R. software.

Acknowledgments—We sincerely appreciate comments regarding this manuscript from Dr. Danuta Kalinowski, Dr. Michael Huang, Dr. Patric Jansson, Dr. Sumit Sahni, Mr. Kyung Chan Park, and Dr. Jan Skoda (Molecular Pharmacology and Pathology Program, Department of Pathology and Bosch Institute, University of Sydney).

References

1. Maruyama, Y., Ono, M., Kawahara, A., Yokoyama, T., Basaki, Y., Kage, M., Aoyagi, S., Kinoshita, H., and Kuwano, M. (2006) Tumor growth suppression in pancreatic cancer by a putative metastasis suppressor gene Cap43/NDRG1/Drg-1 through modulation of angiogenesis. *Cancer Res.* **66,** 6233–6242 CrossRef Medline
2. Kim-Fuchs, C., Winterhalder, S., Winter, A., Malinka, T., Born, D., Schäfer, S., Stroka, D., Gloor, B., Candinas, D., and Angst, E. (2014) The silencing of N-myc downstream-regulated gene-1 in an orthotopic pancreatic cancer model leads to more aggressive tumor growth and metastases. *Dig. Surg.* **31,** 135–142 CrossRef Medline
3. Bandyopadhyay, S., Pai, S. K., Hirota, S., Hosobe, S., Takano, Y., Saito, K., Piquemal, D., Commes, T., Watabe, M., Gross, S. C., Wang, Y., Ran, S., and Watabe, K. (2004) Role of the putative tumor metastasis suppressor gene Drg-1 in breast cancer progression. *Oncogene* **23,** 5675–5681 CrossRef Medline
4. Bandyopadhyay, S., Pai, S. K., Gross, S. C., Hirota, S., Hosobe, S., Miura, K., Saito, K., Commes, T., Hayashi, S., Watabe, M., and Watabe, K. (2003) The Drg-1 gene suppresses tumor metastasis in prostate cancer. *Cancer Res.* **63,** 1731–1736 Medline
5. Guan, R. J., Ford, H. L., Fu, Y., Li, Y., Shaw, L. M., and Pardee, A. B. (2000) Drg-1 as a differentiation-related, putative metastatic suppressor gene in human colon cancer. *Cancer Res.* **60,** 749–755 Medline
6. Kurdistani, S. K., Arizti, P., Reimer, C. L., Sugrue, M. M., Aaronson, S. A., and Lee, S. W. (1998) Inhibition of tumor cell growth by RTP/rit42 and its responsiveness to p53 and DNA damage. *Cancer Res.* **58,** 4439–4444 Medline
7. Kokame, K., Kato, H., and Miyata, T. (1996) Homocysteine-respondent genes in vascular endothelial cells identified by differential display analysis. GRP78/BiP and novel genes. *J. Biol. Chem.* **271,** 29659–29665 CrossRef Medline
8. van Belzen, N., Dinjens, W. N., Diesveld, M. P., Groen, N. A., van der Made, A. C., Nozawa, Y., Vlietstra, R., Trapman, J., and Bosman, F. T. (1997) A novel gene which is up-regulated during colon epithelial cell differentiation and down-regulated in colorectal neoplasms. *Lab. Invest.* **77,** 85–92 Medline
9. Qu, X., Zhai, Y., Wei, H., Zhang, C., Xing, G., Yu, Y., and He, F. (2002) Characterization and expression of three novel differentiation-related genes belong to the human NDRG gene family. *Mol. Cell Biochem.* **229,** 35–44 CrossRef Medline
10. Le, N. T., and Richardson, D. R. (2004) Iron chelators with high antiproliferative activity up-regulate the expression of a growth inhibitory and metastasis suppressor gene: A link between iron metabolism and proliferation. *Blood* **104,** 2967–2975 CrossRef Medline
11. Lane, D. J., Saletta, F., Suryo Rahmanto, Y., Kovacevic, Z., and Richardson, D. R. (2013) N-myc downstream regulated 1 (NDRG1) is regulated by eukaryotic initiation factor 3a (eIF3a) during cellular stress caused by iron depletion. *PLoS One* **8,** e57273 CrossRef Medline
12. Kovacevic, Z., Chikhani, S., Lui, G. Y., Sivagurunathan, S., and Richardson, D. R. (2013) The iron-regulated metastasis suppressor NDRG1 targets NEDD4L, PTEN, and SMAD4 and inhibits the PI3K and Ras signaling pathways. *Antioxid. Redox Signal.* **18,** 874–887 CrossRef Medline
13. Dixon, K. M., Lui, G. Y., Kovacevic, Z., Zhang, D., Yao, M., Chen, Z., Dong, Q., Assinder, S. J., and Richardson, D. R. (2013) Dp44mT targets the AKT, TGF-β and ERK pathways via the metastasis suppressor NDRG1 in normal prostate epithelial cells and prostate cancer cells. *Br. J. Cancer* **108,** 409–419 CrossRef Medline
14. Chen, Z., Zhang, D., Yue, F., Zheng, M., Kovacevic, Z., and Richardson, D. R. (2012) The iron chelators Dp44mT and DFO inhibit TGF-β-induced epithelial-mesenchymal transition via up-regulation of N-Myc downstream-regulated gene 1 (NDRG1). *J. Biol. Chem.* **287,** 17016–17028 CrossRef Medline
15. Jin, R., Liu, W., Menezes, S., Yue, F., Zheng, M., Kovacevic, Z., and Richardson, D. R. (2014) The metastasis suppressor NDRG1 modulates the phosphorylation and nuclear translocation of β-catenin through mechanisms involving FRAT1 and PAK4. *J. Cell Sci.* **127,** 3116–3130 CrossRef Medline
16. Liu, W., Xing, F., Iiizumi-Gairani, M., Okuda, H., Watabe, M., Pai, S. K., Pandey, P. R., Hirota, S., Kobayashi, A., Mo, Y. Y., Fukuda, K., Li, Y., and Watabe, K. (2012) N-myc downstream regulated gene 1 modulates Wnt-β-catenin signalling and pleiotropically suppresses metastasis. *EMBO Mol. Med.* **4,** 93–108 CrossRef Medline
17. Liu, W., Yue, F., Zheng, M., Merlot, A., Bae, D. H., Huang, M., Lane, D., Jansson, P., Lui, G. Y., Richardson, V., Sahni, S., Kalinowski, D., Kovacevic, Z., and Richardson, D. R. (2015) The proto-oncogene c-Src and its downstream signaling pathways are inhibited by the metastasis suppressor, NDRG1. *Oncotarget* **6,** 8851–8874 CrossRef Medline
18. Sun, J., Zhang, D., Zheng, Y., Zhao, Q., Zheng, M., Kovacevic, Z., and Richardson, D. R. (2013) Targeting the metastasis suppressor, NDRG1, using novel iron chelators: Regulation of stress fiber-mediated tumor cell migration via modulation of the ROCK1/pMLC2 signaling pathway. *Mol. Pharmacol.* **83,** 454–469 CrossRef Medline
19. Menezes, S. V., Fouani, L., Huang, M. L. H., Wendimu, B. G., Maleki, S., Richardson, A., Richardson, D. R., and Kovacevic, Z. (2018) The metastasis suppressor, NDRG1, attenuates oncogenic TGF-β and NF-κB signaling to enhance membrane E-cadherin expression in pancreatic cancer cells. *Carcinogenesis*, DOI 10.1093/carcin/bgy178 CrossRef Medline
20. Menezes, S. V., Sahni, S., Kovacevic, Z., and Richardson, D. R. (2017) Interplay of the iron-regulated metastasis suppressor NDRG1 with epidermal growth factor receptor (EGFR) and oncogenic signaling. *J. Biol. Chem.* **292,** 12772–12782 CrossRef Medline
21. Kovacevic, Z., Menezes, S. V., Sahni, S., Kalinowski, D. S., Bae, D. H., Lane, D. J., and Richardson, D. R. (2016) The metastasis suppressor, N-myc downstream-regulated gene-1 (NDRG1), down-regulates the ErbB family of receptors to inhibit downstream oncogenic signaling pathways. *J. Biol. Chem.* **291,** 1029–1052 CrossRef Medline
22. Whitnall, M., Howard, J., Ponka, P., and Richardson, D. R. (2006) A class of iron chelators with a wide spectrum of potent antitumor activity that overcomes resistance to chemotherapeutics. *Proc. Natl. Acad. Sci. U.S.A.* **103,** 14901–14906 CrossRef Medline
23. Sibilia, M., Kroismayr, R., Lichtenberger, B. M., Natarajan, A., Hecking, M., and Holcmann, M. (2007) The epidermal growth factor receptor: From development to tumorigenesis. *Differentiation* **75,** 770–787 CrossRef Medline
24. Burgess, A. W., Cho, H. S., Eigenbrot, C., Ferguson, K. M., Garrett, T. P., Leahy, D. J., Lemmon, M. A., Sliwkowski, M. X., Ward, C. W., and Yokoyama, S. (2003) An open-and-shut case? Recent insights into the activation of EGF/ErbB receptors. *Mol. Cell* **12,** 541–552 CrossRef Medline
25. Zhang, X., Gureasko, J., Shen, K., Cole, P. A., and Kuriyan, J. (2006) An allosteric mechanism for activation of the kinase domain of epidermal growth factor receptor. *Cell* **125,** 1137–1149 CrossRef Medline
26. Zhang, X., Pickin, K. A., Bose, R., Jura, N., Cole, P. A., and Kuriyan, J. (2007) Inhibition of the EGF receptor by binding of MIG6 to an activating kinase domain interface. *Nature* **450,** 741–744 CrossRef Medline
27. Amit, I., Citri, A., Shay, T., Lu, Y., Katz, M., Zhang, F., Tarcic, G., Siwak, D., Lahad, J., Jacob-Hirsch, J., Amariglio, N., Vaisman, N., Segal, E., Rechavi, G., Alon, U., Mills, G. B., Domany, E., and Yarden, Y. (2007) A module of negative feedback regulators defines growth factor signaling. *Nat. Genet.* **39,** 503–512 CrossRef Medline
28. Fry, W. H., Kotelawala, L., Sweeney, C., and Carraway, K. L., 3rd. (2009) Mechanisms of ErbB receptor negative regulation and relevance in cancer. *Exp. Cell Res.* **315,** 697–706 CrossRef Medline
29. Sorkin, A., and Goh, L. K. (2009) Endocytosis and intracellular trafficking of ErbBs. *Exp. Cell Res.* **315,** 683–696 CrossRef Medline
30. Anastasi, S., Sala, G., Huiping, C., Caprini, E., Russo, G., Iacovelli, S., Lucini, F., Ingvarsson, S., and Segatto, O. (2005) Loss of RALT/MIG-6 expression in ERBB2-amplified breast carcinomas enhances ErbB-2 oncogenic potency and favors resistance to Herceptin. *Oncogene* **24,** 4540–4548 CrossRef Medline
31. Xu, D., Makkinje, A., and Kyriakis, J. M. (2005) Gene 33 is an endogenous inhibitor of epidermal growth factor (EGF) receptor signaling and mediates dexamethasone-induced suppression of EGF function. *J. Biol. Chem.* **280,** 2924–2933 CrossRef Medline

32. Wick, M., Bürger, C., Funk, M., and Müller, R. (1995) Identification of a novel mitogen-inducible gene (*mig-6*): Regulation during G_1 progression and differentiation. *Exp. Cell Res.* **219,** 527–535 CrossRef Medline
33. Frosi, Y., Anastasi, S., Ballarò, C., Varsano, G., Castellani, L., Maspero, E., Polo, S., Alemà, S., and Segatto, O. (2010) A two-tiered mechanism of EGFR inhibition by RALT/MIG6 via kinase suppression and receptor degradation. *J. Cell Biol.* **189,** 557–571 CrossRef Medline
34. Yuan, J., Lovejoy, D. B., and Richardson, D. R. (2004) Novel di-2-pyridyl-derived iron chelators with marked and selective antitumor activity: In vitro and in vivo assessment. *Blood* **104,** 1450–1458 CrossRef Medline
35. Kovacevic, Z., Chikhani, S., Lovejoy, D. B., and Richardson, D. R. (2011) Novel thiosemicarbazone iron chelators induce up-regulation and phosphorylation of the metastasis suppressor N-myc down-stream regulated gene 1: A new strategy for the treatment of pancreatic cancer. *Mol. Pharmacol.* **80,** 598–609 CrossRef Medline
36. Lovejoy, D. B., Sharp, D. M., Seebacher, N., Obeidy, P., Prichard, T., Stefani, C., Basha, M. T., Sharpe, P. C., Jansson, P. J., Kalinowski, D. S., Bernhardt, P. V., and Richardson, D. R. (2012) Novel second-generation di-2-pyridylketone thiosemicarbazones show synergism with standard chemotherapeutics and demonstrate potent activity against lung cancer xenografts after oral and intravenous administration in vivo. *J. Med. Chem.* **55,** 7230–7244 CrossRef Medline
37. Li, P., Zheng, X., Shou, K., Niu, Y., Jian, C., Zhao, Y., Yi, W., Hu, X., and Yu, A. (2016) The iron chelator Dp44mT suppresses osteosarcoma's proliferation, invasion and migration: In vitro and in vivo. *Am. J. Transl. Res.* **8,** 5370–5385 Medline
38. Guo, Z. L., Richardson, D. R., Kalinowski, D. S., Kovacevic, Z., Tan-Un, K. C., and Chan, G. C. (2016) The novel thiosemicarbazone, di-2-pyridylketone 4-cyclohexyl-4-methyl-3-thiosemicarbazone (DpC), inhibits neuroblastoma growth in vitro and in vivo via multiple mechanisms. *J. Hematol. Oncol.* **9,** 98 CrossRef Medline
39. Xu, Y. X., Zeng, M. L., Yu, D., Ren, J., Li, F., Zheng, A., Wang, Y. P., Chen, C., and Tao, Z. Z. (2018) *In vitro* assessment of the role of DpC in the treatment of head and neck squamous cell carcinoma. *Oncol. Lett.* **15,** 7999–8004 CrossRef Medline
40. Jansson, P. J., Kalinowski, D. S., Lane, D. J., Kovacevic, Z., Seebacher, N. A., Fouani, L., Sahni, S., Merlot, A. M., and Richardson, D. R. (2015) The renaissance of polypharmacology in the development of anti-cancer therapeutics: Inhibition of the "Triad of Death" in cancer by di-2-pyridylketone thiosemicarbazones. *Pharmacol. Res.* **100,** 255–260 CrossRef Medline
41. Saletta, F., Suryo Rahmanto, Y., Noulsri, E., and Richardson, D. R. (2010) Iron chelator-mediated alterations in gene expression: Identification of novel iron-regulated molecules that are molecular targets of hypoxia-inducible factor-1α and p53. *Mol. Pharmacol.* **77,** 443–458 CrossRef Medline
42. Saarikoski, S. T., Rivera, S. P., and Hankinson, O. (2002) Mitogen-inducible gene 6 (MIG-6), adipophilin and tuftelin are inducible by hypoxia. *FEBS Lett.* **530,** 186–190 CrossRef Medline
43. Park, K. C., Menezes, S. V., Kalinowski, D. S., Sahni, S., Jansson, P. J., Kovacevic, Z., and Richardson, D. R. (2018) Identification of differential phosphorylation and sub-cellular localization of the metastasis suppressor, NDRG1. *Biochim. Biophys. Acta* **1864,** 2644–2663 CrossRef Medline
44. Ghalayini, M. K., Dong, Q., Richardson, D. R., and Assinder, S. J. (2013) Proteolytic cleavage and truncation of NDRG1 in human prostate cancer cells, but not normal prostate epithelial cells. *Biosci. Rep.* **33,** e00042 CrossRef Medline
45. Rojas, M., Yao, S., and Lin, Y. Z. (1996) Controlling epidermal growth factor (EGF)-stimulated Ras activation in intact cells by a cell-permeable peptide mimicking phosphorylated EGF receptor. *J. Biol. Chem.* **271,** 27456–27461 CrossRef Medline
46. Gosney, J. A., Wilkey, D. W., Merchant, M. L., and Ceresa, B. P. (2018) Proteomics reveals novel protein associations with early endosomes in an epidermal growth factor-dependent manner. *J. Biol. Chem.* **293,** 5895–5908 CrossRef Medline
47. Carpenter, G., and Liao, H. J. (2009) Trafficking of receptor tyrosine kinases to the nucleus. *Exp. Cell Res.* **315,** 1556–1566 CrossRef Medline
48. Richardson, D. R., and Baker, E. (1994) Two saturable mechanisms of iron uptake from transferrin in human melanoma cells: The effect of transferrin concentration, chelators, and metabolic probes on transferrin and iron uptake. *J. Cell Physiol.* **161,** 160–168 CrossRef Medline
49. Longva, K. E., Blystad, F. D., Stang, E., Larsen, A. M., Johannessen, L. E., and Madshus, I. H. (2002) Ubiquitination and proteasomal activity is required for transport of the EGF receptor to inner membranes of multivesicular bodies. *J. Cell Biol.* **156,** 843–854 CrossRef Medline
50. Futter, C. E., Pearse, A., Hewlett, L. J., and Hopkins, C. R. (1996) Multivesicular endosomes containing internalized EGF-EGF receptor complexes mature and then fuse directly with lysosomes. *J. Cell Biol.* **132,** 1011–1023 CrossRef Medline
51. Nishimura, Y., Yoshioka, K., Bereczky, B., and Itoh, K. (2008) Evidence for efficient phosphorylation of EGFR and rapid endocytosis of phosphorylated EGFR via the early/late endocytic pathway in a gefitinib-sensitive non-small cell lung cancer cell line. *Mol. Cancer* **7,** 42 CrossRef Medline
52. Seebacher, N. A., Lane, D. J., Jansson, P. J., and Richardson, D. R. (2016) Glucose modulation induces lysosome formation and increases lysosomotropic drug sequestration via the P-glycoprotein drug transporter. *J. Biol. Chem.* **291,** 3796–3820 CrossRef Medline
53. Chu, F. Y., Haley, S. C., and Zidovska, A. (2017) On the origin of shape fluctuations of the cell nucleus. *Proc. Natl. Acad. Sci. U.S.A.* **114,** 10338–10343 CrossRef Medline
54. Huynh, K. K., Eskelinen, E. L., Scott, C. C., Malevanets, A., Saftig, P., and Grinstein, S. (2007) LAMP proteins are required for fusion of lysosomes with phagosomes. *EMBO J.* **26,** 313–324 CrossRef Medline
55. Dunn, K. W., Kamocka, M. M., and McDonald, J. H. (2011) A practical guide to evaluating colocalization in biological microscopy. *Am. J. Physiol. Cell Physiol.* **300,** C723–C742 CrossRef Medline
56. Park, E., Kim, N., Ficarro, S. B., Zhang, Y., Lee, B. I., Cho, A., Kim, K., Park, A. K. J., Park, W. Y., Murray, B., Meyerson, M., Beroukhim, R., Marto, J. A., Cho, J., and Eck, M. J. (2015) Structure and mechanism of activity-based inhibition of the EGF receptor by Mig6. *Nat. Struct. Mol. Biol.* **22,** 703–711 CrossRef Medline
57. Darnell, G., and Richardson, D. R. (1999) The potential of iron chelators of the pyridoxal isonicotinoyl hydrazone class as effective antiproliferative agents III: The effect of the ligands on molecular targets involved in proliferation. *Blood* **94,** 781–792 Medline
58. Liang, S. X., and Richardson, D. R. (2003) The effect of potent iron chelators on the regulation of p53: Examination of the expression, localization and DNA-binding activity of p53 and the transactivation of WAF1. *Carcinogenesis* **24,** 1601–1614 CrossRef Medline
59. Fiorini, M., Ballarò, C., Sala, G., Falcone, G., Alemà, S., and Segatto, O. (2002) Expression of RALT, a feedback inhibitor of ErbB receptors, is subjected to an integrated transcriptional and post-translational control. *Oncogene* **21,** 6530–6539 CrossRef Medline
60. Shinde, S. R., and Maddika, S. (2016) PTEN modulates EGFR late endocytic trafficking and degradation by dephosphorylating Rab7. *Nat. Commun.* **7,** 10689 CrossRef Medline
61. Kalinowski, D. S., and Richardson, D. R. (2005) The evolution of iron chelators for the treatment of iron overload disease and cancer. *Pharmacol. Rev.* **57,** 547–583 CrossRef Medline
62. Stacy, A. E., Palanimuthu, D., Bernhardt, P. V., Kalinowski, D. S., Jansson, P. J., and Richardson, D. R. (2016) Structure-activity relationships of di-2-pyridylketone, 2-benzoylpyridine, and 2-acetylpyridine thiosemicarbazones for overcoming Pgp-mediated drug resistance. *J. Med. Chem.* **59,** 8601–8620 CrossRef Medline
63. Richardson, D., Ponka, P., and Baker, E. (1994) The effect of the iron(III) chelator, desferrioxamine, on iron and transferrin uptake by the human malignant melanoma cell. *Cancer Res.* **54,** 685–689 Medline
64. Ferby, I., Reschke, M., Kudlacek, O., Knyazev, P., Pantè, G., Amann, K., Sommergruber, W., Kraut, N., Ullrich, A., Fässler, R., and Klein, R. (2006) Mig6 is a negative regulator of EGF receptor-mediated skin morphogenesis and tumor formation. *Nat. Med.* **12,** 568–573 CrossRef Medline
65. Wang, Y. (2010) Breast cancer metastasis driven by ErbB2 and 14–3-3zeta: A division of labor. *Cell Adh. Migr.* **4,** 7–9 CrossRef Medline
66. Morgan, E. H. (1981) Inhibition of reticulocyte iron uptake by NH4Cl and CH3NH2. *Biochim. Biophys. Acta* **642,** 119–134 CrossRef Medline

67. Paterson, S., Armstrong, N. J., Iacopetta, B. J., McArdle, H. J., and Morgan, E. H. (1984) Intravesicular pH and iron uptake by immature erythroid cells. *J. Cell Physiol.* **120,** 225–232 CrossRef Medline
68. Pietiäinen, V., Vassilev, B., Blom, T., Wang, W., Nelson, J., Bittman, R., Bäck, N., Zelcer, N., and Ikonen, E. (2013) NDRG1 functions in LDL receptor trafficking by regulating endosomal recycling and degradation. *J. Cell Sci.* **126,** 3961–3971 CrossRef Medline
69. Lee, K. H., Choi, E., Chun, Y. S., Kim, M. S., and Park, J. W. (2006) Differential responses of two degradation domains of HIF-1α to hypoxia and iron deficiency. *Biochimie* **88,** 163–169 CrossRef Medline
70. Lee, J. C., Chiang, K. C., Feng, T. H., Chen, Y. J., Chuang, S. T., Tsui, K. H., Chung, L. C., and Juang, H. H. (2016) The iron chelator, Dp44mT, effectively inhibits human oral squamous cell carcinoma cell growth in vitro and in vivo. *Int. J. Mol. Sci.* **17,** E1435 CrossRef Medline
71. Xi, R., Pun, I. H., Menezes, S. V., Fouani, L., Kalinowski, D. S., Huang, M. L., Zhang, X., Richardson, D. R., and Kovacevic, Z. (2017) Novel thiosemicarbazones inhibit lysine-rich carcinoembryonic antigen-related cell adhesion molecule 1 (CEACAM1) coisolated (LYRIC) and the LYRIC-induced epithelial-mesenchymal transition via upregulation of N-myc downstream-regulated gene 1 (NDRG1). *Mol. Pharmacol.* **91,** 499–517 CrossRef Medline
72. Liu, W., Kovacevic, Z., Peng, Z., Jin, R., Wang, P., Yue, F., Zheng, M., Huang, M. L., Jansson, P. J., Richardson, V., Kalinowski, D. S., Lane, D. J., Merlot, A. M., Sahni, S., and Richardson, D. R. (2015) The molecular effect of metastasis suppressors on Src signaling and tumorigenesis: New therapeutic targets. *Oncotarget* **6,** 35522–35541 CrossRef Medline
73. Lui, G. Y., Kovacevic, Z., Menezes, S. V., Kalinowski, D. S., Merlot, A. M., Sahni, S., and Richardson, D. R. (2015) Novel thiosemicarbazones regulate the signal transducer and activator of transcription 3 (STAT3) pathway: inhibition of constitutive and interleukin 6-induced activation by iron depletion. *Mol. Pharmacol.* **87,** 543–560 CrossRef Medline
74. Accornero, P., Miretti, S., Starvaggi Cucuzza, L., Martignani, E., and Baratta, M. (2010) Epidermal growth factor and hepatocyte growth factor cooperate to enhance cell proliferation, scatter, and invasion in murine mammary epithelial cells. *J. Mol. Endocrinol.* **44,** 115–125 CrossRef Medline
75. Krall, J. A., Beyer, E. M., and MacBeath, G. (2011) High- and low-affinity epidermal growth factor receptor-ligand interactions activate distinct signaling pathways. *PLoS One* **6,** e15945 CrossRef Medline
76. Richardson, D. R., Sharpe, P. C., Lovejoy, D. B., Senaratne, D., Kalinowski, D. S., Islam, M., and Bernhardt, P. V. (2006) Dipyridyl thiosemicarbazone chelators with potent and selective antitumor activity form iron complexes with redox activity. *J. Med. Chem.* **49,** 6510–6521 CrossRef Medline
77. Gao, J., and Richardson, D. R. (2001) The potential of iron chelators of the pyridoxal isonicotinoyl hydrazone class as effective antiproliferative agents, IV: The mechanisms involved in inhibiting cell-cycle progression. *Blood* **98,** 842–850 CrossRef Medline
78. Fu, D., and Richardson, D. R. (2007) Iron chelation and regulation of the cell cycle: 2 mechanisms of posttranscriptional regulation of the universal cyclin-dependent kinase inhibitor p21CIP1/WAF1 by iron depletion. *Blood* **110,** 752–761 CrossRef Medline